TEAMER Post Access Report

Project Title: Numerical Modeling, Analysis, and Optimization of Oscillo-Drive Wave Energy Converter

Awardee: Wave Water Works LLC

Awardee point of contact: Peter Bailey, pbailey@wavewaterworksusa.com

Facility: Florida Atlantic University

Facility point of contact: Professor Manhar Dhanak, dhanak@fau.edu

Date: July 17, 2026

EXECUTIVE SUMMARY

The primary objective of this project is to optimize the Oscillo-Drive Wave Energy Converter (WEC) system developed by Wave Water Works. This system, designed for low-wattage applications such as recharging buoys and emergency equipment, captures wave energy and converts it into mechanical and electrical power. The focus of the project is to enhance the efficiency of energy conversion by refining six key system parameters: arm length, float radius, float mass, generator damping coefficient, geartrain ratio, and flywheel inertia.

To work towards this objective, the project will employ advanced numerical modeling and simulation techniques. WEC-Sim, an open-source tool developed by the National Renewable Energy Laboratory (NREL) and Sandia National Laboratories, will be used to simulate the dynamic interaction between the WEC and incoming waves. The simulations will focus on optimizing the energy capture process, taking into account wave characteristics and the WEC's mechanical design.

The modeling process will involve several steps:

1. **Design and CAD Modeling**: The WEC system geometry, including the float and arm, will be modeled using SolidWorks. The design will reflect the system's interaction with typical wave fields.
2. **Mesh Generation**: A high-quality finite element mesh of the system will be generated using CUBIT, ensuring accurate simulation of the WEC's hydrodynamic behavior.
3. **Hydrodynamic Analysis**: Hydrodynamic forces acting on the float will be calculated using NEMOH, a Boundary Element Method (BEM) tool. These coefficients, such as added mass and radiation damping, will be used to simulate wave-induced forces on the float.
4. **Numerical Simulation in WEC-Sim**: Time-domain simulations will be run in WEC-Sim to analyze the WEC's motion and energy conversion under varying wave conditions. The simulations will model key components, such as the PTO system and generator, to ensure accurate power output predictions.
5. **Parameter Optimization**: A parameter sweep will be conducted to systematically vary arm length, float size, and other factors. The goal is to identify the combination of parameters that maximizes both mechanical and electrical power output.

The project will ensure that each step is carefully executed to provide insights into how different system configurations affect the overall performance of the WEC.

1 INTRODUCTION TO THE PROJECT

The goal of this project is to optimize the performance of Wave Water Works' Oscillo Drive Wave Energy Converter (WEC) system. The current focus is on small-scale applications, such as recharging capabilities for data buoys and emergency position-indicating radio beacons (EPIRB). This work involves modeling the conversion of wave energy into mechanical energy and, crucially, the subsequent conversion of mechanical power into electrical power through an integrated generator. By simulating the system with varying parameters—including float arm length, float size, gear ratio, flywheel inertia, and generator characteristics—the project aims to determine the optimal configurations for maximizing power output while ensuring practical scalability for low-wattage marine applications. This work will support future designs for larger-scale applications by ensuring the cost-effective development of a viable, small-scale product.

2 Roles and Responsibilities of Project Participants

2.1 Applicant Responsibilities and Tasks Performed

Wave Water Works (WWW) has developed the small-scale prototype of the Oscillo Drive wave energy converter (WEC) system. Their responsibilities include:

- Providing detailed technical specifications and performance data for the current prototype.
- Outlining the key parameters of interest for optimization (e.g., arm length, float size, generator damping coefficient, gear ratio, flywheel mass).
- Supplying physical prototypes and materials needed for testing.
- Collaborating with FAU during the optimization process to ensure the design improvements align with practical considerations.

2.2 Network Facility Responsibilities and Tasks Performed

Florida Atlantic University (FAU), as the network facility, is responsible for conducting the optimization study. Tasks include:

- Simulating the WEC system in varying wave environments to assess the impact of different design parameters on mechanical and electrical power output.
- Modeling the complete power conversion chain, including the generator dynamics, to ensure realistic energy capture assessments.
- Performing parameter sweeps and rerunning BEM for different arm lengths and float sizes as required.
- Analyzing the results to provide recommendations for optimizing the WEC for different environmental conditions and power requirements.
- Providing technical reports on the findings, along with any additional insights for the improvement of the generator and float arm design.

3 Project Objectives

Overall Objective: The primary objective of this project is to optimize the Oscillo-Drive Wave Energy Converter (WEC) system to enhance the efficiency of converting wave energy into electrical power. This includes refining system parameters such as the float, arm, gear ratio, flywheel, and generator, with a focus on maximizing energy conversion over a range of sea states. The project aims to develop a fully optimized wave-to-wire model that integrates both mechanical and electrical power generation. For Wave Water Works (WWW), the optimization of the Oscillo-Drive WEC system is critical to advancing their device from a proof-of-concept prototype to a commercially viable product. Improved efficiency and performance will allow WWW to better target low-wattage, off-grid applications such as recharging systems for buoys and emergency equipment. This project will provide WWW with the data and insights needed to further develop their system, making it more competitive in the renewable energy market.

Physical Attributes to Investigate: The optimization will focus on the following key physical attributes:

- Float: Diameter, shape, and mass of the float
- Arm: Length and stiffness of the arm connecting the float to the system
- Flywheel: Mass and inertia of the flywheel to store rotational energy
- Gear Ratio: The gear ratio between the float's mechanical motion and the generator input
- Generator: Damping coefficient and electrical power generation efficiency
- Wave Conditions: Regular and irregular wave profiles modeled using the Pierson-Moskowitz spectrum.

Performance Metrics: The performance of the optimized Oscillo-Drive WEC system will be evaluated using the following metrics:

- Mechanical Power Output: The power generated by the float-arm system before electrical conversion.
- Electrical Power Output: The power produced by the generator as a function of the mechanical power input.
- Energy Conversion Efficiency: The ratio of electrical power output to the total available wave energy.
- Optimization of WEC Response: Performance of the WEC in capturing energy over a wide range of wave frequencies and amplitudes.

4 Test Facility, Equipment, Software, and Technical Expertise

The following resources will be used to execute the proposed optimization study:

- High-Performance Computing (HPC) Resources: FAU has access to HPC resources that will allow the team to perform computationally expensive simulations and optimizations efficiently.
- WEC-Sim and Boundary Element Method (BEM) Models: WEC-Sim [1, 2] will be used to simulate the system's hydrodynamic response and interactions with waves. BEM models will provide the necessary hydrodynamic coefficients, such as added mass, damping, and restoring forces. Tools like NEMOH (see, for example, [3]) will be used to generate these coefficients.
- MATLAB Optimization Tools: MATLAB's fmincon function will be used for constrained optimization, and global optimization techniques like genetic algorithms

will also be considered. These will handle the non-linear nature of the problem and constraints on system parameters.

- WecOptTool [4]: This tool, designed specifically for optimizing WEC designs by Sandia Labs, will be explored as an alternative or complement to WEC-Sim for performing high-dimensional optimization studies more efficiently.
- SolidWorks for CAD design of WEC components.
- CUBIT for mesh models.
- NEMOH for hydrodynamic coefficient calculation.
- Technical Expertise: FAU provides a team of engineers and researchers with expertise in marine energy, hydrodynamic modeling, mechanical and electrical engineering, and optimization processes. Wave Water Works (WWW), the applicant, brings deep knowledge of their prototype system and will work closely with FAU throughout the project.
- Ocean Test Site Conditions: Simulations will model realistic wave conditions based on data collected from three selected locations with different wave characteristics.

5 Test or Analysis Article Description

Technology Overview: The technology under investigation is the Oscillo-Drive Wave Energy Converter (WEC), developed by Wave Water Works (WWW). The Oscillo-Drive WEC harnesses ocean wave energy and converts it into electrical power. Its primary components include a float connected to an arm, a geartrain, a flywheel, and a generator. This system utilizes the oscillatory motion of waves to drive mechanical motion in the arm and float, which is then transferred through a gear system to the generator to produce electrical energy.

WWW has, for many years, been building a variety of prototype models of the Oscillo Drive patented device. The “O”-Drive technology is totally scalable across a myriad of applications and power ranges. With an eye on the economy of scale and available resources, it was thought prudent to develop the WEC for smaller, low wattage applications rather than shooting for the moon in the early phases of development.

Recently, we have been designing and building small prototypes for lower power applications where the WEC could provide, for example, recharging capability for data collection and transmission such as required by instrumentation buoys (based on discussions with NOAA in Ann, Arbor, Michigan), and emergency position-indicating radio beacons (EPIRB) for search and rescue efforts, life rafts, and personal watercraft (based on discussions with representatives from the US Coast Guard). There are numerous other applications for devices with low wattage power generation capabilities. Developing a successful device for this range of power could be achieved more quickly and economically, while reaching commercial viability more rapidly.

Our current device (Figs. 1-3) is approximately the size of a shoebox. It incorporates our patented “O”-Drive with a single input or float arm of approximately 3-4 feet in length having a float attached that is roughly the size of a soccer ball or a beach ball. The internal shafts are 12mm in diameter and the gears are modified, COTS (commercial-off-the-shelf), 1.5 mod x 15mm face width stainless steel gears with a total 25:1 output ratio to the flywheel. The flywheel is derived from a simple three spoke cast iron handwheel that is turned and balanced. Current, non-optimized flywheel weight is approximately 2.5 lbs. This will require some study for efficiency in design.

Electrical and Control Properties: The flywheel is connected to a core-less generator which has a 50 Watt capacity and can run at speeds as low as 250 RPM. This small generator is not the ideal generator, but there are currently few options in the low RPM realm. Very little research and development has taken place for low RPM generators since there are few applications where a generator would not be driven by a much higher RPM motor or engine.

There have been significant advances of late in core-less motor development which utilize PCB's for stacking many, thin layers of coils on stacked layer printed circuit boards and permanent magnet rotors. This same concept can be used for generators as well. By using these PCB stators, many can be interleaves with thin rotors to generate much greater output at lower RPM's. We have built one such generator using wire-wound coils and have used the purchased core-less generator mentioned previously with some success. With more study and optimization, we believe we can build our own generators to greatly enhance not only the physical size of the generator, but also the performance.

Our gear case design is a split gearbox for easy assembly and was 3D printed from PLA material. The commercialized version will have an injection molded case with proper gasket seals for environmental integrity. The reciprocating input shaft connected to the float arm and float, both requiring optimization study, is captured with a rubber boot to allow the oscillating motion while maintaining a waterproof capsule.
In terms of control, the system employs a simple damping control strategy that regulates the resistance provided by the generator to the mechanical input from the float and arm. This control ensures that the WEC operates at its optimal point across a range of wave conditions. During the optimization process, advanced control algorithms may be tested to further improve the system's ability to adapt to different wave frequencies and amplitudes.

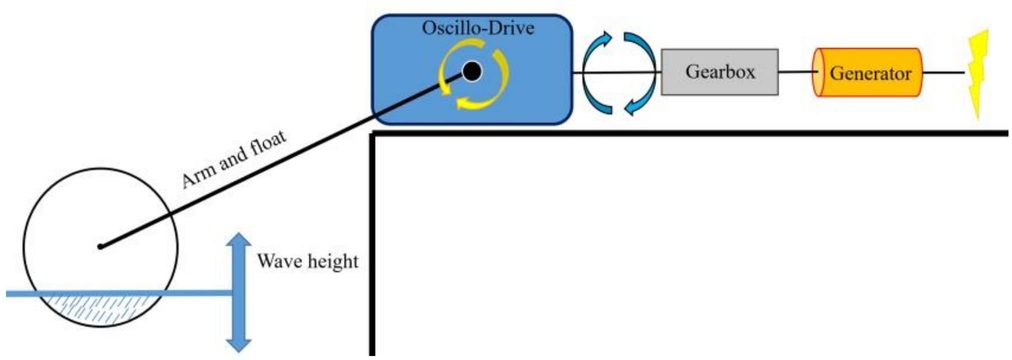

Fig. 1. Schematic of the system concept

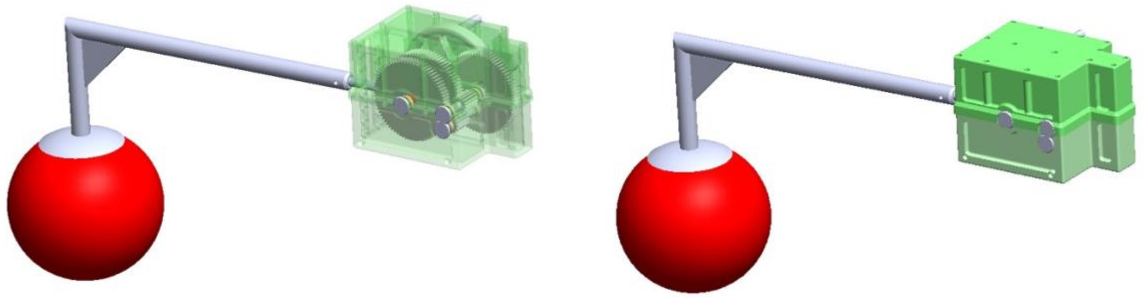

Fig. 1a. Schematics of the current Oscillo Drive WEC

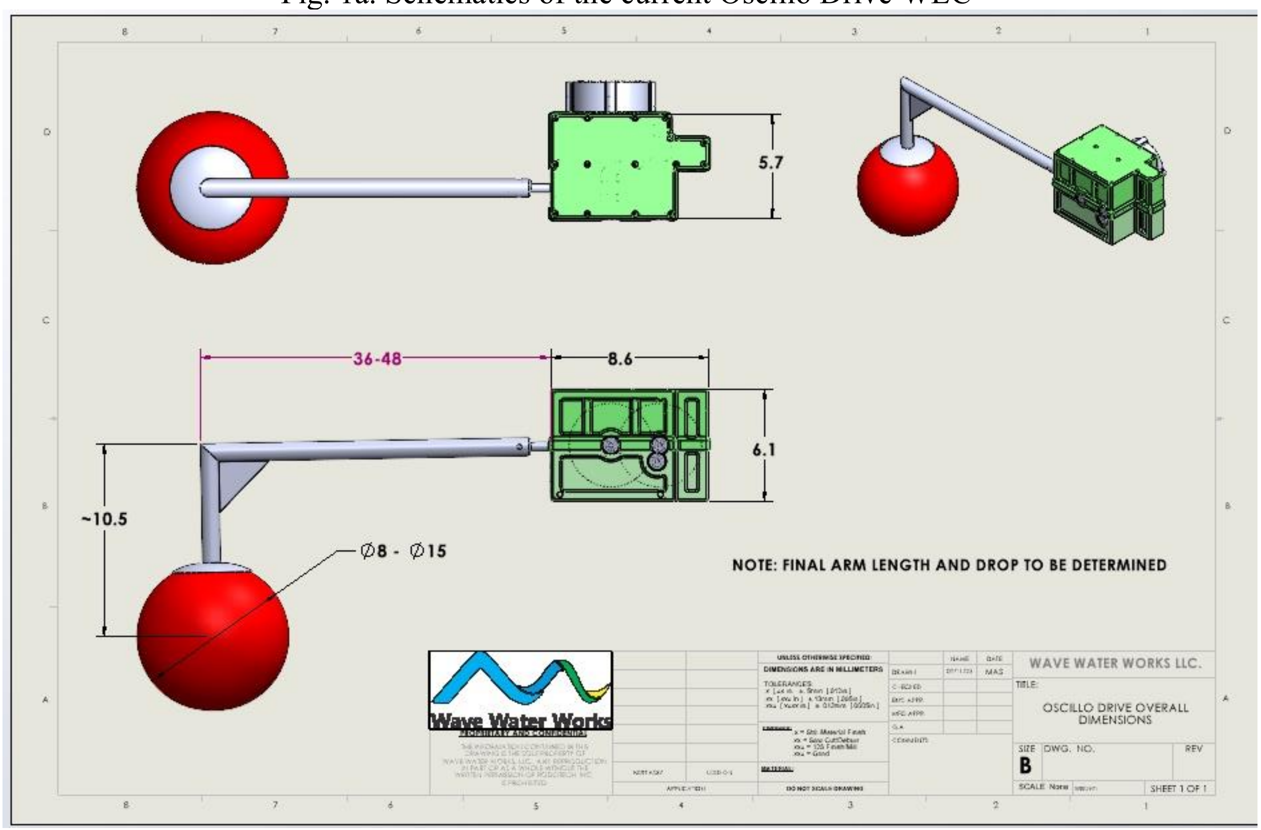

Fig. 2. Physical dimensions (in inches) of the system

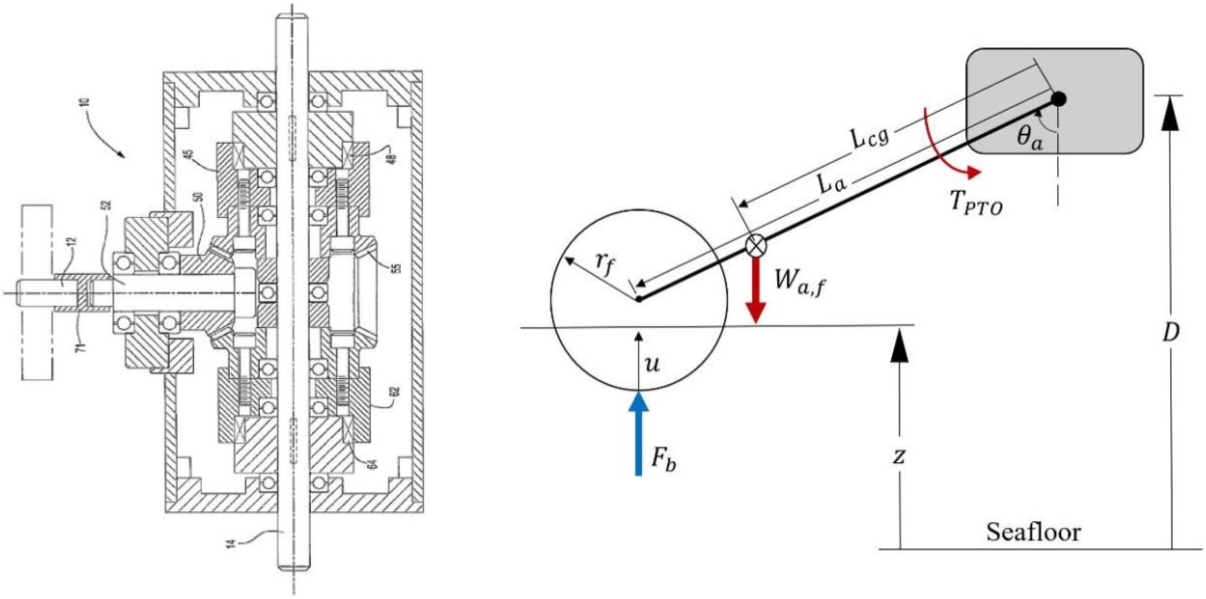

Fig. 3. Left: Section view taken from the Oscillo-Drive patent; Right: Force diagram of WEC

Parameter Sweep: An outline of the parameter sweep process is as follows: Systematically vary key WEC parameters such as arm length, float radius, float mass, generator damping coefficient, geartrain ratio, and flywheel inertia to explore their individual and combined effects on mechanical and electrical power output. Each parameter will be adjusted within predefined ranges based on practical constraints and expected operational conditions. For each configuration, the corresponding hydrodynamic coefficients will be recalculated using Boundary Element Method (BEM) analysis to ensure that the effects of parameter variations on wave-structure interactions are fully accounted for. The objective is to identify the optimal combination of these parameters that maximizes the mechanical energy conversion under varying wave conditions. As described above, the WEC scale and wave conditions to be considered are:

WEC scale: The scale will primarily depend on the local dominant wavelength and height of the incident waves. As an initial choice for the simulation, we will consider incident waves of length 8 – 10m and wave heights in the range 0.2 – 0.5m. These represent moderate ocean waves typically associated with longer period swell. While the wave height will be a key factor in power conversion, the wavelength also influences the choice of arm length, as the float will experience varying wave conditions over each wave cycle. Correspondingly, we will choose a spherical float of diameter 0.22m (size of a soccer ball) and an arm length in the range 2 – 3m. For the small size of the float, a longer arm is needed to take advantage of the wave's potential energy over its cycle. However, the arm length should not be too long, as otherwise the small float size might limit energy capture if the arm is too disproportionate. Initial choices for the other key parameters would be based on the existing system: float mass: 10kg; the gear ratio: 1:30; generator damping coefficient: 0.65 N.s/m; flywheel inertia: 0.1 kg.m^2. These parameters will be adjusted based on simulation results and further testing. A balance between energy capture efficiency and mechanical feasibility will be key in finalizing the optimal values of the parameters.
Wave conditions: A combination of regular, irregular, low-energy, high-energy, and location-specific wave fields will be targeted in the analysis and optimization process. A

Pierson-Moskowitz spectrum will be used in simulation to model irregular waves. These wave conditions will help provide a holistic understanding of how the Oscillo-Drive WEC performs across different environments under real-world conditions. Prevalent wave-conditions at the three test site locations will be determined, in terms of dominant wave heights and wave periods, and will guide considerations.

The primary objective of this study is to optimize the WEC parameters related to the conversion of wave energy into mechanical energy, as this stage represents the core of the energy capture process. While mechanical power alone may not fully reflect the overall performance of a WEC, it provides valuable insights into how the system efficiently harnesses wave energy before losses associated with energy conversion take place.

That said, we acknowledge the importance of considering the entire power conversion chain, including the impact of the generator. The generator imposes a load on the system, influencing the mechanical energy output. To account for this, the model will include the generator's effect through an equivalent damping coefficient, which approximates its impact on energy conversion. This approach simplifies the model while still capturing the essential dynamics of the system, offering a practical way to assess performance. Given that the optimization process primarily targets mechanical power output for design and parameter tuning, this simplified modeling approach is both relevant and effective. It allows us to maintain clarity and feasibility in evaluating the WEC's performance while acknowledging the generator's influence.

However, since the necessary tools to consider the conversion from wave to wire are available, we will extend the proposed study to include a more detailed model incorporating generator dynamics and control strategies in assessing performance in the conversion of wave to mechanical to electrical power.

6 Work Plan

The work plan consists of several phases designed to address the computational and technical challenges outlined by the reviewers, including the need to model both mechanical and electrical power output:

<u>Phase 1: Preliminary Study (1-2 months)</u>

- Perform an initial assessment using WEC-Sim to determine the influence of wave height and other wave conditions on power output. This will help refine the list of optimization variables and potentially reduce the computational complexity of the multivariate optimization.
- Evaluate the need to include wave height in the optimization based on this initial analysis.

<u>Phase 2: Hydrodynamic Modeling and System Simulation (3-4 months)</u>

- Develop a hydrodynamic model using Nemoh to generate the necessary hydrodynamic coefficients based on system parameters (float radius, arm length, etc.).

- Simulate the WEC's response to various wave conditions using WEC-Sim. Regular and irregular waves (Pierson-Moskowitz spectrum) will be modeled, and the effects of float geometry, mass, and arm length will be explored.
- Ensure the frequency variation of the hydrodynamic coefficients is captured accurately to estimate power production appropriately, as per Reviewer 1's suggestion.

<u>Phase 3: Optimization Study (3-5 months)</u>

- Use MATLAB's fmincon function and genetic algorithms to perform the initial optimization of mechanical power output. The optimization process will systematically vary key parameters (float size, arm length, etc.) to find the configuration that maximizes power output.
- Explore WecOptTool as a potential alternative for high-parameter optimization, as recommended by Reviewer 1 and 3. This tool may help reduce computational costs by handling complex multivariate optimizations more efficiently.
- Expand the optimization process to incorporate generator dynamics and extend the study to optimize electrical power output.

<u>Phase 4: Validation and Refinement (2-3 months)</u>

- Validate the optimization results through additional simulations and, if possible, physical testing.
- Perform sensitivity analysis to evaluate how the optimized parameters influence overall system performance under different wave conditions.
- Refine the optimization process based on feedback and further testing.

<u>Phase 5: Final Report and Dissemination (1-2 months)</u>

- Prepare a final report documenting the optimized design, methodology, and results.
- Disseminate findings to stakeholders and the broader marine energy community, highlighting the broader impact of the methodological framework developed for WEC optimization.

6.1 Numerical Model Description

The numerical analysis will be conducted using WEC-Sim, an open-source wave energy converter simulation tool developed by the National Renewable Energy Laboratory (NREL) and Sandia National Laboratories. WEC-Sim simulates the hydrodynamic interaction between the WEC components (float, arm, and PTO system) and incoming waves to predict performance and enable optimization.

Workflow and Simulation Setup: The design process begins with creating the basic CAD geometry of the Oscillo-Drive WEC in SolidWorks, followed by meshing the float using Sandia Lab's CUBIT. The mesh is pre-processed using the Boundary Element Method (BEM) tool NEMOH, which computes hydrodynamic coefficients based on linear potential flow wave theory. The resulting output file is converted to an .h5 format using WEC-Sim's BEMIO (Boundary Element Method Input Output) and fed into the WEC-Sim model.

WEC-Sim will then simulate the dynamic response of the WEC under varying wave conditions, with outputs including velocity, acceleration, forces, and mechanical power. The model will represent the Oscillo-Drive's input shaft as a fixed pivot point above the water level, with an arm extending toward the incoming waves. The float, attached to the arm's end, will capture wave-induced forces and convert them into mechanical energy through the PTO system.

Key Parameters for Optimization: To maximize the conversion of wave energy to mechanical and electrical energy, we will optimize several key parameters:

- Arm Length: Adjusted to optimize mechanical leverage and the forces exerted by the waves.
- Float Size and Mass: The float's radius and mass will be tuned to enhance buoyancy and maximize wave energy capture.
- PTO System: The generator damping coefficient will be modeled to optimize the mechanical-to-electrical conversion, ensuring energy transfer efficiency.
- Geartrain Ratio: This affects the speed-torque conversion, influencing the mechanical energy transfer to the generator.
- Flywheel Inertia: Helps stabilize power output by smoothing mechanical fluctuations caused by wave variability.

Hydrodynamic and Mechanical Modeling: The Boundary Element Method (BEM) analysis will capture the hydrodynamic interaction of the float with incoming waves, including wave-induced forces, added mass, and radiation damping. These coefficients will be fed into WEC-Sim to simulate the dynamic response of the system. The float mesh will be refined until hydrodynamic coefficients converge, ensuring the mesh density is optimized for accurate simulation results. Pierson-Moskowitz wave spectrum will be used to simulate irregular sea states, modeling wave height, period, and direction over a 10-minute simulation time.

The entire process will involve iterative sweeps of parameter changes (float size, arm length, damping coefficients, etc.), with reruns of BEM simulations to capture updated hydrodynamic coefficients. This iterative process ensures accurate simulation results, particularly in terms of optimizing the system for different wave conditions and configurations.

Optimization of Mechanical and Electrical Conversion: Beyond mechanical energy optimization, the model will also incorporate the generator dynamics to evaluate **wave-to-wire** energy conversion. The PTO system will include an equivalent damping coefficient representing the generator's load on the system, allowing the simulation to reflect how mechanical energy is converted to electrical energy. This holistic approach provides a clear understanding of the WEC's overall performance, from wave energy capture to the generation of electrical power.

The simulation will focus on maximizing both mechanical power output (captured by the float and converted by the PTO) and electrical power output (considering the generator's efficiency and energy transfer dynamics).

Numerical Methods and Validation:

- Mesh and Time Step Studies: A mesh study will be conducted to ensure that the computational grid used in the simulation provides accurate hydrodynamic solutions without excessive computational cost. Time-step sensitivity will also be evaluated to balance solution accuracy and efficiency.
- Boundary Conditions: The wave tank conditions will be replicated in the simulation by carefully selecting boundary conditions, such as wave height, period, and direction, which will reflect real-world marine conditions.
- Validation: The numerical model will be validated using data from previous small-scale experiments on the Oscillo-Drive WEC. This will involve comparison between simulated power output and experimental results under similar wave conditions, ensuring that the numerical predictions are reliable.

Previous Studies: The accuracy of WEC-Sim has been validated through multiple studies, which have benchmarked the software against experimental wave tank data for various WEC designs.

This integrated process, combining BEM analysis, numerical modeling, and generator dynamics, will allow for a detailed optimization of the Oscillo-Drive WEC. The focus will be on maximizing both mechanical and electrical energy outputs, making the system more efficient and viable for real-world marine energy applications.

Detailed Technical Steps:

Step 1: Design and CAD Modeling in SolidWorks. The initial WEC geometry, including the arm length and float dimensions, will be designed in SolidWorks. The 3D model will focus on the interaction between the spherical float and the arm, ensuring that the geometry accounts for hydrodynamic behavior under varying wave conditions. This CAD model will serve as the foundation for later hydrodynamic and mechanical analysis.

Step 2: Mesh Generation Using CUBIT. After designing the model in SolidWorks, a finite element mesh will be generated using CUBIT. Special attention will be paid to refining the mesh around the float, as its interaction with waves is critical for accurate simulations. The mesh density will be optimized until the hydrodynamic coefficients converge, ensuring that the simulation results are accurate without excessive computational cost.

Step 3: Hydrodynamic Coefficients Calculation in NEMOH. NEMOH, a Boundary Element Method (BEM) tool, will compute hydrodynamic coefficients such as added mass, radiation damping, and excitation forces acting on the float in various wave fields. Reruns of the BEM simulations will be performed for each configuration of arm length and float radius to ensure accuracy in parameter sweeps. The computed coefficients will be converted into .h5 files and fed into WEC-Sim via BEMIO.

Step 4: Numerical Simulation and Optimization in WEC-Sim. The dynamic response of the WEC will be simulated using WEC-Sim, focusing on optimizing several key parameters, including the generator damping coefficient, geartrain ratio, and flywheel inertia. These simulations will be conducted under various wave conditions to maximize mechanical power. The optimization process will employ techniques like genetic algorithms or gradient-based methods to identify the optimal combination of parameters for maximizing energy output.

Step 5: Parameter Sweep and Optimization. A parameter sweep will systematically vary key WEC parameters (arm length, float radius, mass, generator damping coefficient, geartrain ratio, and flywheel inertia) within predefined ranges. The impact of these changes on mechanical power output will be measured through rerunning hydrodynamic simulations (using NEMOH) and dynamic simulations (using WEC-Sim). The aim is to optimize the system for maximum mechanical power output and energy conversion efficiency.

6.2 TEST AND ANALYSIS MATRIX AND SCHEDULE

To optimize the Oscillo-Drive WEC, a series of simulations and physical tests will be performed. The matrix below outlines the key parameters that will be varied during the tests and simulations, as well as the corresponding timeline.

Test/Analysis	Parameters to Vary	Purpose	Expected Timeline
Phase 1: Preliminary Study	Wave conditions	To determine the influence of wave height and other wave conditions on power output	Weeks 1-6
Phase 2: Hydrodynamic Modeling and System Simulation	Float size, arm length, PTO damping	To generate the hydrodynamic coefficients, and evaluate WEC performance as parameters are varied	Weeks 1-16
Phase 3: Optimization Study	Float size, arm length, PTO damping, gear ratio	To optimize for mechanical and electric power output	Weeks 4 - 20
Phase 4: Validation and Refinement	Wave conditions from 3 selected locations for 2 target power productions	To validate the optimization results and provide assessment of performance in real world conditions	Weeks 15 - 25
Phase 5: Final Report and Dissemination	-	To Prepare a final report documenting the optimized design, methodology, and results.	Weeks 22 - 28

The numerical simulations will help identify the best parameter ranges for the physical tests, and feedback from the applicant will further refine the optimization.

6.3 DATA MANAGEMENT, PROCESSING, AND ANALYSIS

6.3.1 Data Management

All data generated during the project will be securely stored at FAU’s High-Performance Computing (HPC) Center, which will provide both local storage and backup services. The data structure will include raw simulation data, processed test results, and metadata describing the experimental conditions and parameter settings for each test.

The data submission will be handled as follows:

Data Type	Format	Submission to MHK DR
Numerical Simulation Data	.mat (MATLAB), .h5	Yes
Optimized WEC Parameters	.csv, .txt	Yes

Data will be structured according to FAU's internal guidelines, ensuring clear traceability and reproducibility.

6.3.2 Data Processing

The data collected during both the numerical will be processed as follows: Results from WEC-Sim simulations will be post-processed using MATLAB scripts to extract key performance metrics such as power output, efficiency, and energy capture across different wave conditions.

7 Project Outcomes

7.1 Results

The schematic of the modeled point-absorber wave energy converter (WEC) is shown in Fig. 1. A light rigid moment arm of length L_{arm} connects a spherical float of diameter d to the power take-off (PTO) shaft. The heaving motion of the float caused by incident waves is transmitted through the arm to the PTO shaft. In the absence of waves, the float is in static equilibrium with a submerged depth h with corresponding float mass of

$$m(h) = \rho V (\frac{h}{d})^2 \left(3 - \frac{2h}{d}\right),$$

where V is the volume of the sphere, determined from Archimedes' principle by equating the float weight to the buoyant force associated with the displaced water volume.

The study considered five float diameters, d = 0.15, 0.20, 0.30, 0.40, and 0.50 m. For each diameter, three equilibrium submergence levels, corresponding to progressively increasing float masses, were examined as listed in Table 1. This resulted in a total of 15 unique float geometry and mass configurations being evaluated.

Submerged depth, h	**Fraction of full sphere mass (ρV)**
$0.25d$	$5/32$
$0.50d$	$1/2$
$0.75d$	$27/32$

Table 1. Submergence level/float mass cases considered.

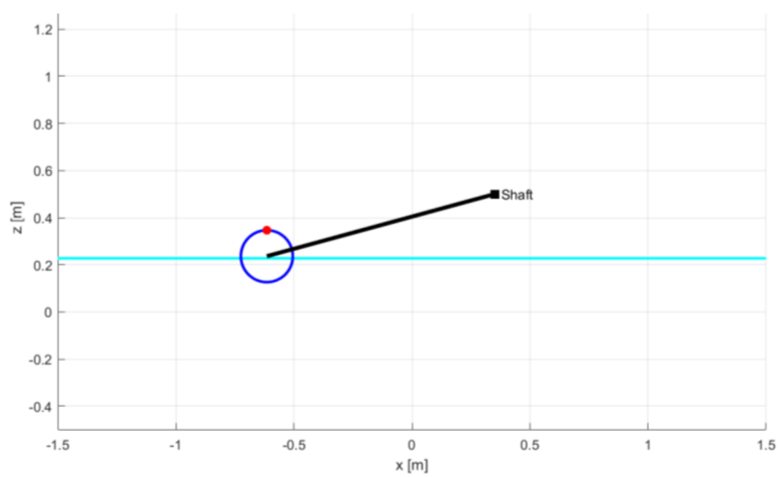

Fig. 1. Schematics of the modeled point-absorber WEC

The system's behavior is dictated by the geometric constraint:

$$(x_c - x_{sp})^2 + (z_c - z_{sp})^2 = L_{arm}^2$$

where (x_c, z_c) is the instantaneous position of the float center and (x_{sp}, z_{sp}) is the fixed position of the PTO shaft.

Upon completing the float geometry in SolidWorks, the design was exported as an STL file and converted into high-resolution surface meshes appropriate for boundary element method (BEM) solvers. Custom Python scripts were developed to facilitate the meshing and conversion process with the Capytaine hydrodynamic solver. To achieve adequate accuracy in subsequent simulations, mesh resolution was controlled using user-defined parameters, which determine the number of subdivisions in the azimuthal and polar directions on the sphere surface. n_θ was generally set to 60, and $n_\phi$was set to 30. This led to a well-refined mesh that demonstrated smooth curvature and satisfactory element aspect ratios (Fig. 2).

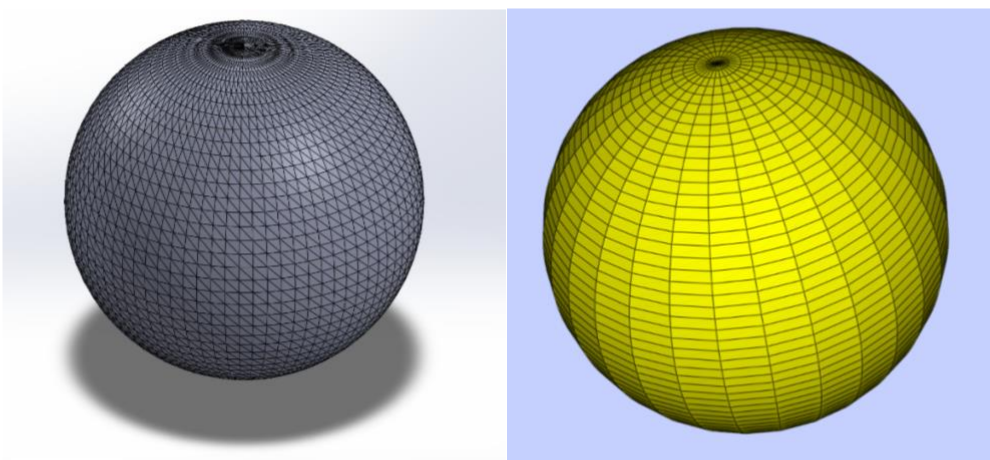

Fig. 2. STL and aligned Capytaine meshes of the spherical float.

The study considered five float diameters, d = 0.15, 0.20, 0.30, 0.40, and 0.50 m. For each diameter, four equilibrium submergence levels were examined as listed in Table 1. This resulted in a total of 20 unique float geometry and mass configurations being evaluated.

After the surface mesh generation, alignment with the global coordinate system was executed to ensure accurate motion response in the heave and to maintain consistency with WEC-Sim protocols. Subsequently, the aligned mesh was exported in the NetCDF(.nc) format, which functioned as the standard input for Capytaine simulations.

Hydrodynamic coefficients for time-domain simulation were calculated using Capytaine, an open-source boundary element method (BEM) solver that functions in the frequency domain. A Python workflow was used for the analysis, assigning the defined spherical float mesh to a Floating Body object along with its physical properties. The BEMSolver class in Capytaine computes frequency-dependent added mass and radiation damping coefficients by addressing the hydrodynamic boundary value problem over a specified range of wave frequencies. The normalized heave added mass, $\frac{A_{33}}{M}$, heave radiation damping, $\frac{B_{33}}{\omega M}$, and response amplitude operator (RAO), $|\frac{\zeta}{A}|$ were determined for across all values of the diameter d and shown to collapse onto single curves when plotted as functions of the dimensionless frequency parameter, $s = \frac{\omega^2 d}{g}$ for each value of submergence depth h. This is consistent with dimensional analysis as for infinite water depth we have

$$\frac{A_{33}}{M} = F_1\left(\frac{\omega^2 d}{g}\right); \frac{B_{33}}{\omega M} = F_2\left(\frac{\omega^2 d}{g}\right); \left|\frac{\zeta}{A}\right| = F_3\left(\frac{\omega^2 d}{g}\right).$$

Here $M(= \rho V_{disp})$ is the mass of the float-arm system, ω is the frequency of the incident wave, and A is its amplitude. Figs. 3-5 present the resulting normalized added mass, radiation damping, and RAO curves for the three retained submergence ratios as functions of the non-dimensional frequency parameter, $s = \frac{\omega^2 d}{g}$.

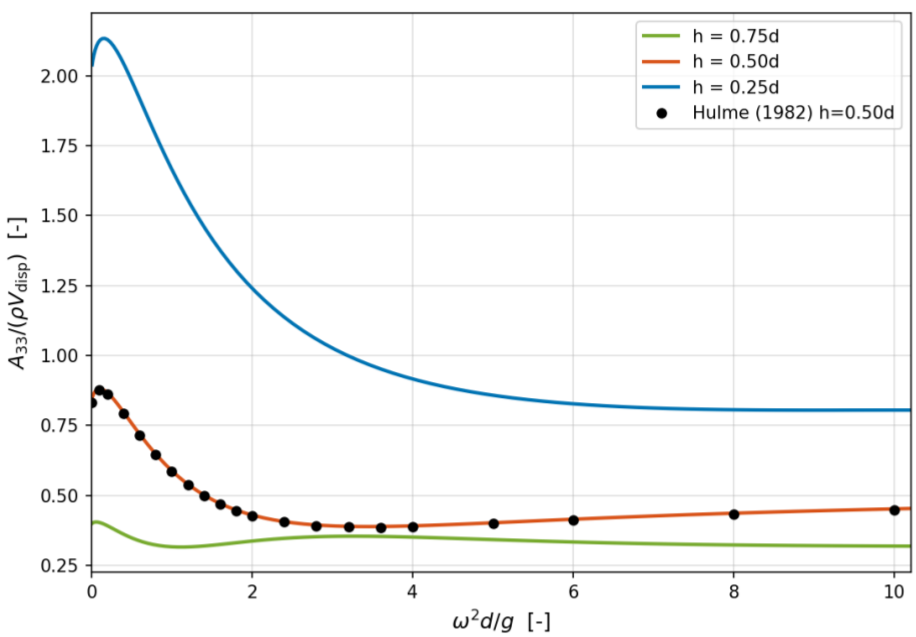

Fig. 3. Normalized heave added mass vs. $\frac{\omega^2 d}{g}$ for h/d = 0.75, 0.50, 0.25

A mesh-convergence study (600–2400 panels per case) confirmed these normalized added-mass curves are resolved to better than 1% away from isolated irregular-frequency points, and the h/d = 0.50 curve matches Hulme's (1982) exact semi-analytic solution for a floating hemisphere to within 0.5% across the full frequency range shown, validating the panel resolution and body geometry used throughout this sweep.

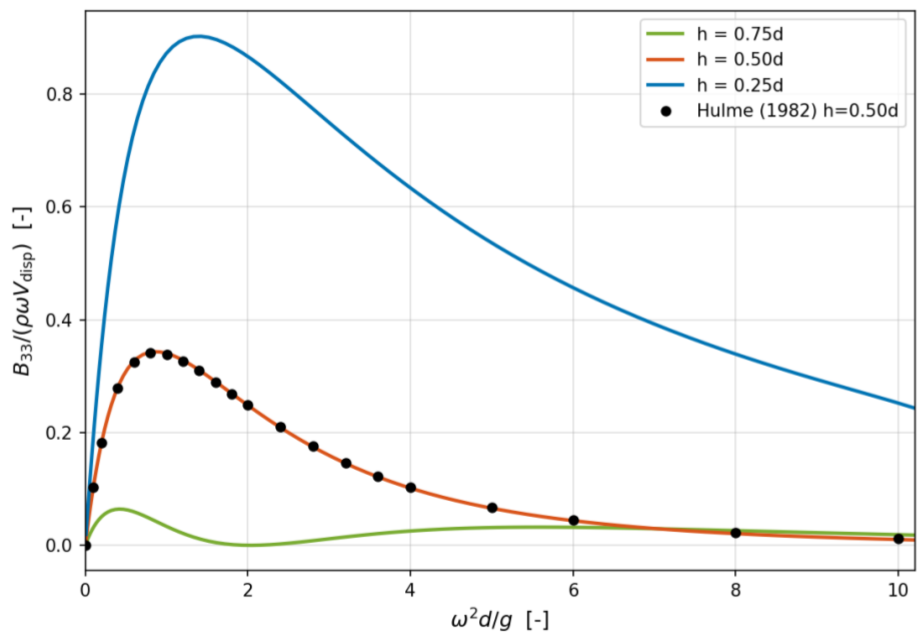

Fig. 4. Normalized heave radiation damping vs. $\frac{\omega^2 d}{g}$ for h/d = 0.75, 0.50, 0.25

The BEM-based normalized heave damping (Fig. 4) for the case $h = 0.5d$ matches Hulme (1982) to within about 1%. The normalized heave radiation heave damping peak values of 0.065, 0.34 and 0.90 respectively for h/d = 0.75, 0.50 and 0.25.

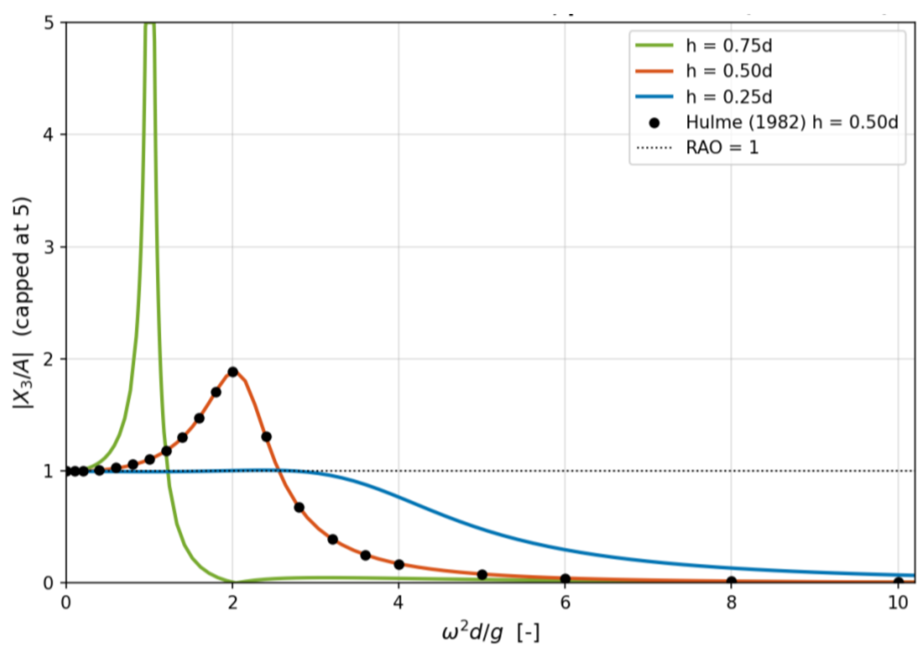

Fig. 5. Normalized heave RAO vs. $\frac{\omega^2 d}{g}$ for h/d = 0.75, 0.50, 0.25

The case $h = 0.75d$ has the highest RAO peak value (RAO ≈ 11.3) at $\frac{\omega^2 d}{g} = 1.01$, confirming this case is the most lightly damped of the three cases considered and therefore the most susceptible to large resonant amplification absent added damping. It is important to note that Figs. 3-5 reflect radiation and diffraction hydrodynamics only: no viscous drag or PTO damping is included, so the true in-service response — particularly the sharp h/d = 0.75 peak — will be lower once these additional loss mechanisms are present.

As an illustration of this effect, Figs. 6–7 show the impact of adding an idealized, impedance-matched (resistance-only) power take-off (PTO) damping term, $B_{33,PTO}(\omega) = \sqrt{(B_{33}^2 + (K/\omega)^2)}$, where $K = C_{33} - \omega^2(m + A_{33})$, computed independently at each frequency to maximize instantaneous absorbed power. This represents the theoretical upper bound on what a purely resistive PTO can achieve at each frequency in isolation — not a realizable fixed-parameter controller — but it usefully brackets how far the resonant peaks above can be tamed by damping alone.

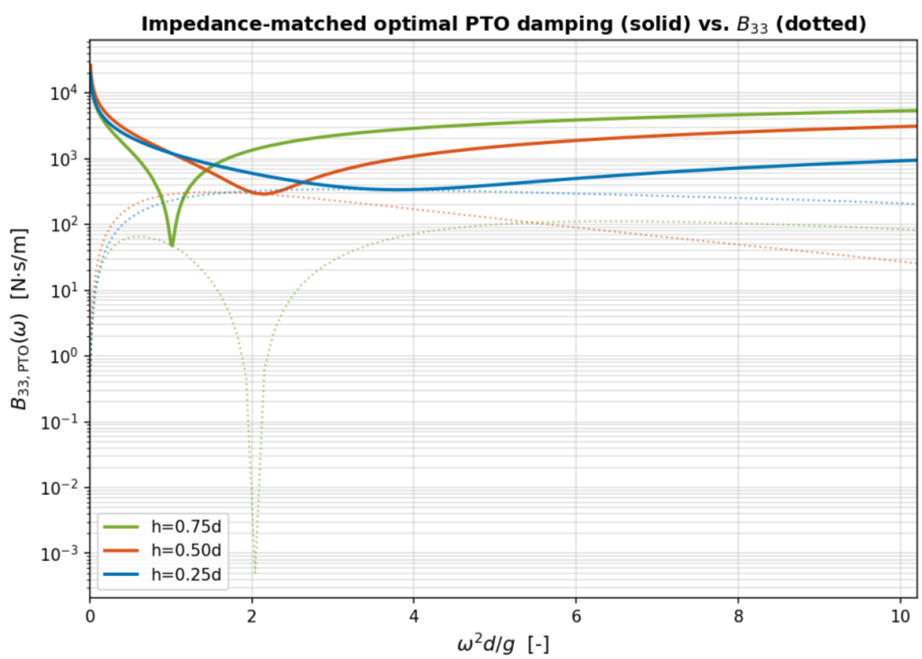

Fig. 6. Impedance-matched optimal PTO damping $B_{33,PTO}(\omega)$ vs. $B_{33}(\omega)$, h/d = 0.75, 0.50, 0.25.

The optimal damping equals B_{33} exactly at each case's own resonance (where K = 0) and rises sharply away from it, where most of the added ‘damping’ is in fact reactive compensation for the stiffness-inertia mismatch rather than genuine dissipation; at the h/d = 0.75 resonance, only about 48 N·s/m of added damping — comparable to B_{33} there — is needed to reach the impedance-matched optimum.

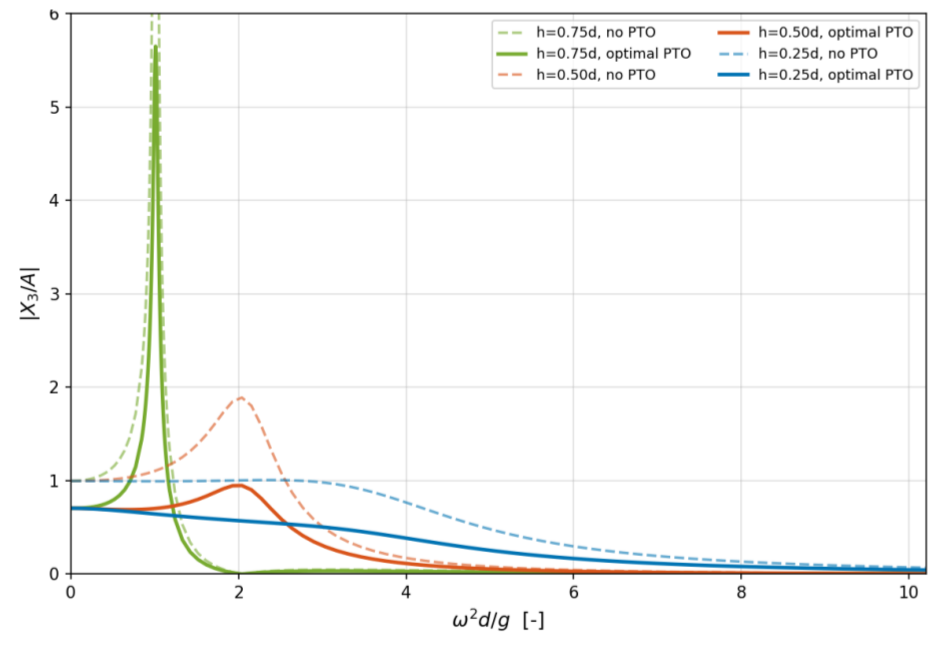

Fig. 7. Heave RAO with vs. without impedance-matched optimal PTO damping, h/d = 0.75, 0.50, 0.25

Because total damping exactly doubles at each resonance under this scheme, all three peak RAO values are cut almost exactly in half (h/d = 0.75: 11.3 → 5.6; h/d = 0.50: 1.9 → 0.9; h/d = 0.25: 1.0 → 0.7), while the curves away from resonance are comparatively unaffected. This confirms that PTO damping is most effective, per unit of damping added, precisely at resonance — reinforcing the case for tuning the PTO load to track each design's natural frequency rather than applying a fixed damping value across all sea states.

The RAO curves (Fig. 5) reveal a clear resonance hierarchy: the h/d = 0.75 case exhibits a sharp, lightly-damped resonance peak (RAO ≈ 11.3) near $\omega^2 d/g \approx 1$; the h/d = 0.50 case shows a broader, more moderate peak (RAO ≈ 1.9) near $\omega^2 d/g \approx 2$; and the h/d = 0.25 case shows no distinct resonance peak in this range, instead following the incident wave (RAO ≈ 1) up to $\frac{\omega^2 d}{g} \approx 4$ before declining. This hierarchy provided the basis for a refined optimization in which the float mass M was directly tied to the equilibrium displaced volume ($M = \rho V_{disp}$) for each submergence ratio, and the diffraction- and Froude-Krylov-consistent excitation force computed by Capytaine was used directly (rather than back-calculated from a target RAO). A self-consistency check confirmed that the resulting model reproduces Capytaine's own RAO output, validating the interpolation, non-depersonalization, and Froude-rescaling pipeline (Fig. 8).

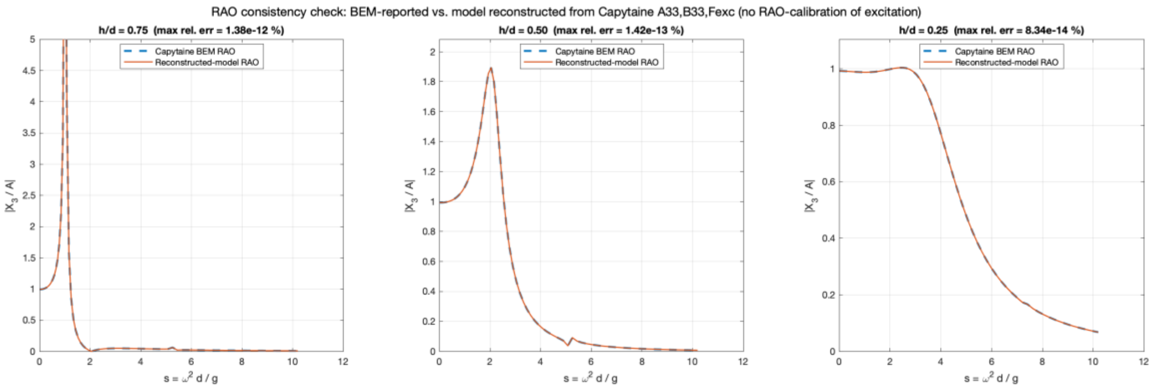

Fig. 8. RAO consistency check: Capytaine BEM RAO vs. reconstructed-model RAO
(h/d = 0.75, 0.50, 0.25)

7.1.1 WEC-Sim Simulation

The wave energy converter was dynamically simulated in the time domain using WEC-Sim, a MATLAB Simulink-based program specifically designed to describe the interactions between ocean waves and floating objects. The system under consideration was modeled as a single body configuration, representing a partially submerged spherical float that was constrained to heaving motion, thereby permitting vertical translation only. Hydrodynamic data, which includes frequency-dependent added mass, radiation damping, and wave excitation forces, were precomputed in Capytaine and then imported into WEC-Sim using the .h5 file generated via the BEMIO interface. The governing equation of motion, derived from the Cummins formulation, includes contributions from wave excitation, radiation forces, restoring force, additional mass, viscous damping, and a linear PTO damper. Before executing the simulation, a custom Simulink model was developed using the block library offered by WEC-Sim. The arrangement included the hydrodynamic body block, wave block, PTO block, and mechanical reference and constraint blocks, arranged to enable the simulation of vertical movement exclusively.

The wave conditions considered in this study, including both regular and irregular waves, are summarized in Table 2.

Case	***Wave Type***	***Wave Height (H/Hs)***	***Wave Period (T/Top)***
Reg1	Regular	0.5 m	3 s
Reg2	Regular	0.5 m	7 s
SS1	Irregular	0.5 m (Hs)	3 s (Tp)
SS2	Irregular	1.0 m (Hs)	7 s (Tp)
SS3	Irregular	1.5 m (Hs)	9 s (Tp)

Table 2. Wave conditions studied.

The computations were executed for a duration of 400 seconds. The initial 100 seconds constituted a ramp phase that facilitated the system's attainment of steady-state waves. A fixed step 4th-order Runge-Kutta solution was employed with a 0.01 second increment to ensure numerical stability. The simulated wave and wave-induced heaving motion for case $h = 0.5d$ are shown in Figs. In Figs. 9-11. The data in Fig. 9 illustrates the fluctuations in the height of the wave surface as time progresses. The profile shows a rising trend in wave amplitude during the ramp period, followed by a steady periodic behavior, providing reliable external forcing to the WEC.

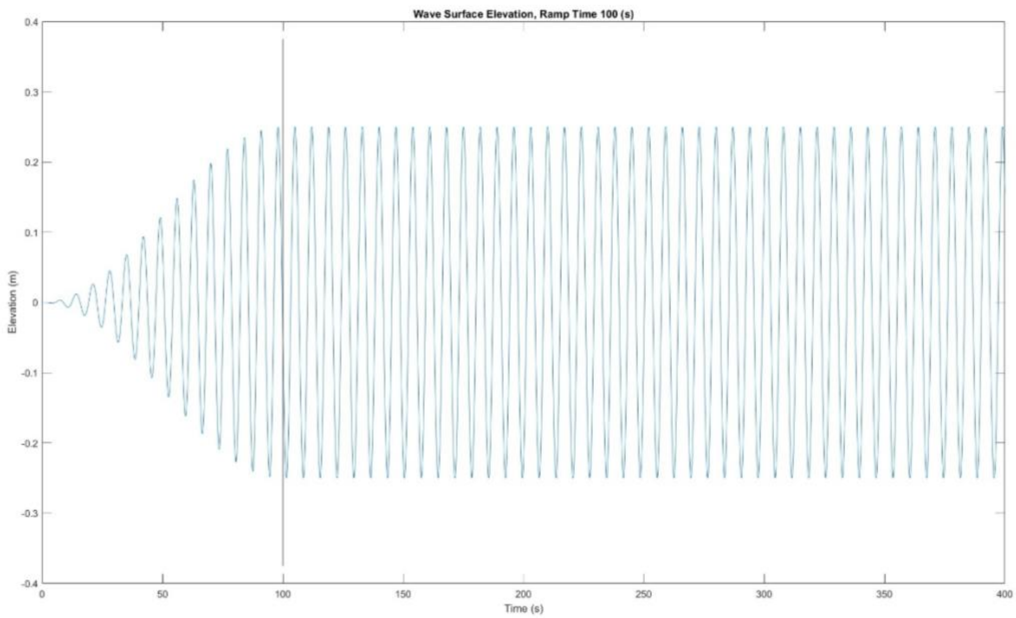

Fig. 9. Wave surface elevation over time showing ramp-up and steady-state behavior under regular wave conditions for the case $h = 0.5d$.

As the wave forcing advances, the spherical float demonstrates a dynamic response in heave. The comprehensive hydrodynamic force exerted on the float is comprised of several components, each linked to a specific physical phenomenon. The components consist of wave excitation, radiation damping, added mass, hydrostatic restoring forces, and viscous damping forces. The decomposition of the force components is depicted in Fig. 10, which illustrates their relative magnitudes and phasing during the simulation process. The primary oscillatory behavior is predominantly governed by excitation and restoring forces, whereas the transient and steady-state response is affected by the damping and added mass terms. The symmetry and smooth periodicity of these forces serve as indicators of model stability and hydrodynamic consistency.

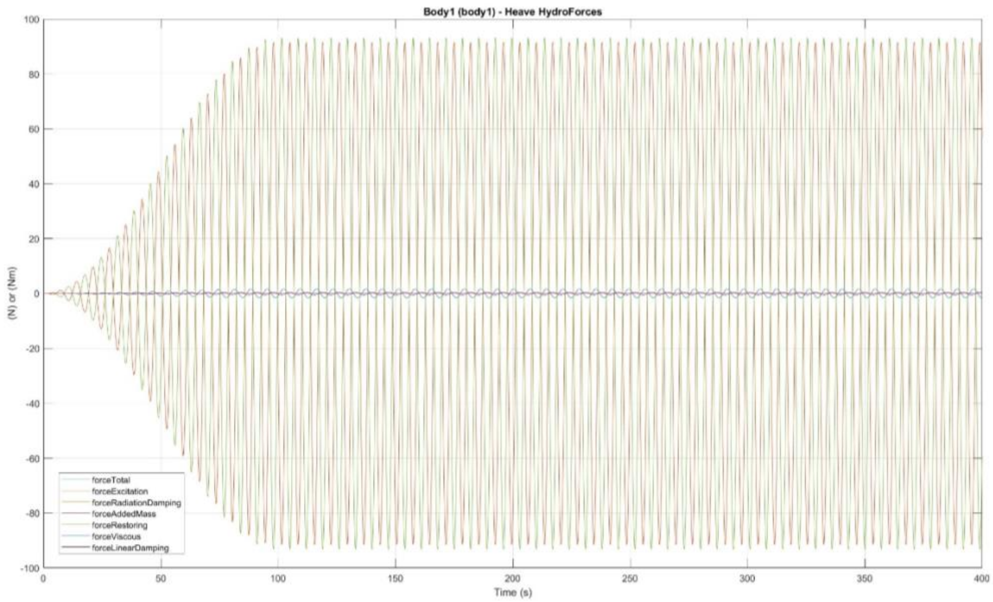

Fig. 10. Decomposition of hydrodynamic heave forces acting on the float for case $h = 0.5d$

The time-domain response related to the float is illustrated in Fig. 11, showcasing the position, velocity, and acceleration in the heave direction. Following the initial ramp-up phase, the system reaches a condition of periodic motion that aligns with the incident wave field. The amplitude and frequency of the response align with the anticipated dynamics for a system exhibiting a resonant frequency close to the wave frequency, thereby confirming the accurate integration of mass, stiffness, and damping parameters within the model. The velocity and acceleration traces demonstrate a phase shift concerning position, consistent with the principles of harmonic motion, and can be employed for estimating absorbed power during post-processing analysis.

The simulation outputs were accompanied by a visualization generated through the SimMechanics Explorer, which is integrated within WEC-Sim. This instrument offers a three-dimensional visualization of the Wave Energy Converter (WEC) system throughout the time-domain simulation, facilitating the assessment of model configuration, body dynamics, and wave interactions within the spatial domain.

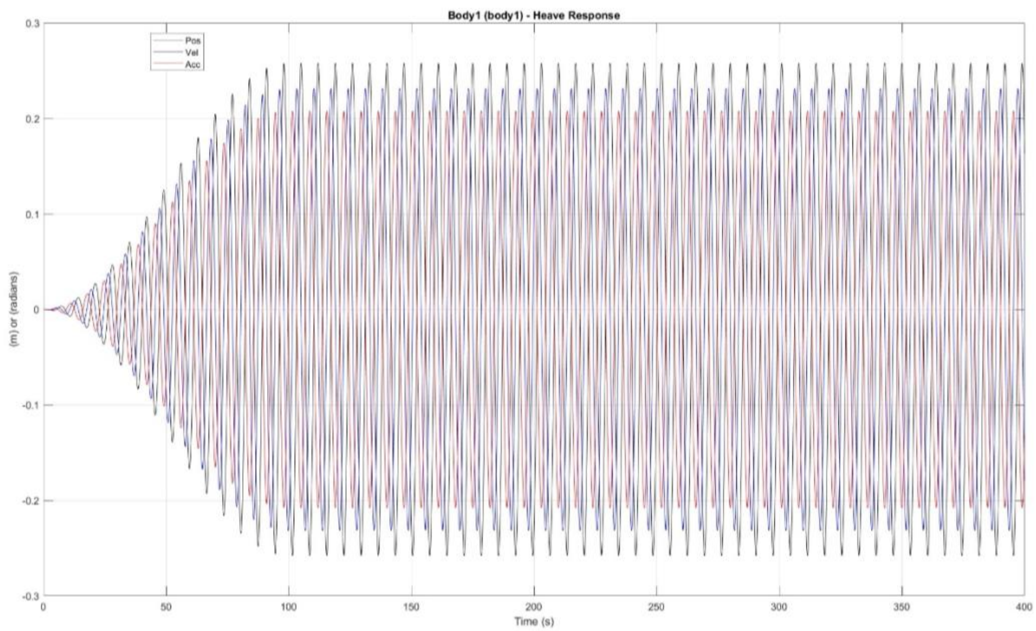

Fig. 11. Heave displacement, velocity, and acceleration of the float, showing convergence to periodic steady-state motion after ramp time for case $h = 0.5d$

7.1.2 Optimization and Power Analysis

The optimization framework was utilized to assess the performance of the wave energy converter over a spectrum of geometric and operational parameters, including the float diameter d, arm length L_{arm}, first for the submergence level of $h = 0.5d$ and PTO load. The findings are delineated for both standard wave conditions and irregular sea states to evaluate the design's robustness and to ascertain the key factors affecting energy absorption. While hydrodynamic coefficients were obtained for multiple submergence configurations, the optimization results and corresponding power maps presented in this section are based on the half-submerged case. Selected results are presented to avoid redundancy and improve the interpretability of the optimization trends.

The PTO and generator parameters used in the optimization are listed in Table 7.2. These are based on a specific generator /PTO configuration currently being considered for the WEC. However, these may change as improved low-RPM generator becomes available.

Parameter	*Value*	*Description*
G	63.5	Gear ratio
J fly	0.01 kg m^2	Flywheel inertia
R gen	5.0 Ω	Generator internal resistance
Ke	0.212 V/(rad/s)	Back-EMF constant
Kt	0.212 N m/A	Torque constant
B mech hinge	0.0 N m s/rad	Mechanical hinge damping

Table 3. PTO/generator parameters considered.

The power maps (Figs. 12, 13) obtained for regular wave conditions show that the absorbed power is not governed by float diameter or arm length independently, but by their combined interaction. The plots identify confined regions of favorable design combinations rather than a uniform improvement with increasing size. This indicates that the system response depends on geometric tuning with respect to the excitation condition, rather than simple scaling of dimensions. In the scenario concerning the shorter wave period, $T = 3s$ (Reg1), the optimal region is identified as being centered around a diameter of approximately 0.20 m and an arm length of 0.60 m, at which point the system attains its maximum power output. In the context of the longer wave period, $T = 7s$ (Reg2), the optimal configuration shifts to a different geometric configuration, specifically around a diameter of 0.25 m and an arm length of 0.60 m. This shift confirms that the optimal geometry is strongly dependent on wave frequency, and that different excitation conditions require different geometric configurations for effective energy capture.

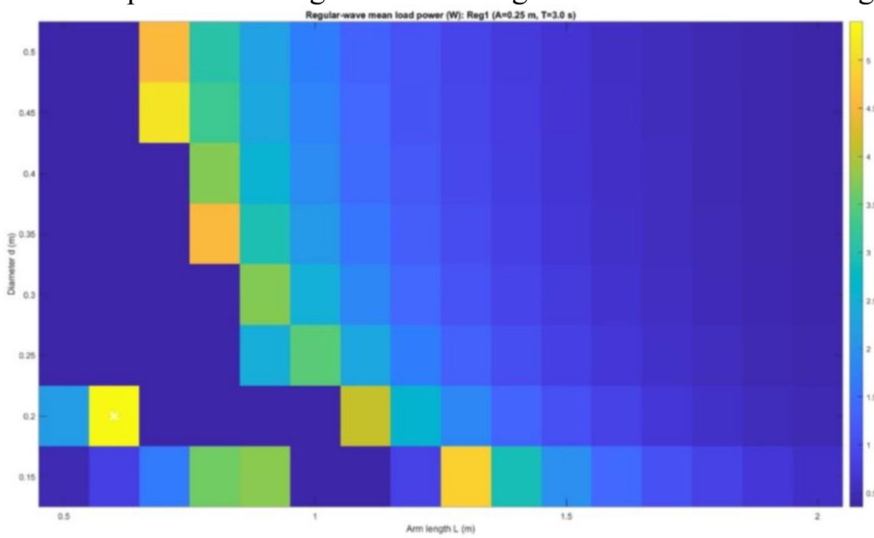

Fig. 12. Regular-wave power map (Reg1) for case $h = 0.5d$. The color bar indicates electric power generated in Watts,

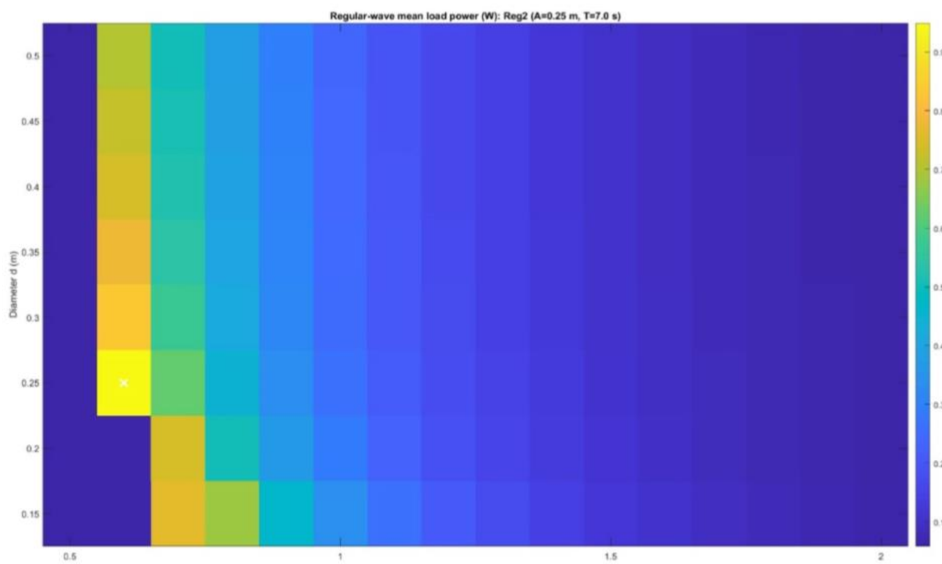

Fig. 13. Regular-wave power map (Reg2) for case $h = 0.5d$. The color bar indicates electric power generated in Watts.

A comparison of these regular-wave results shows that a geometry optimized for one wave condition does not remain optimal for another. This behavior reflects the frequency-dependent balance between excitation forces, radiation damping, hydrostatic restoring effects, and PTO loading. The regular-wave analysis, therefore, demonstrates that the converter operates as a tuned system, where geometry must be selected in accordance with the dominant wave characteristics.

The irregular-wave power map (Fig. 14) extends this analysis to realistic sea-state conditions, where the device is subjected to a distribution of wave frequencies rather than a single harmonic input. The results in Fig. 14 show that the optimal configuration corresponds to diameter $d = 0.5\ m$ and arm length $L_{arm} = 0.6$ m for irregular wave conditions related to SS1. The implication of this result is that optimization based solely on regular-wave response is inadequate for practical design, as the presence of a wave spectrum modifies the effective operating conditions of the device. The analysis of irregular waves underscores the necessity of assessing performance in realistic sea states to determine resilient design parameters.

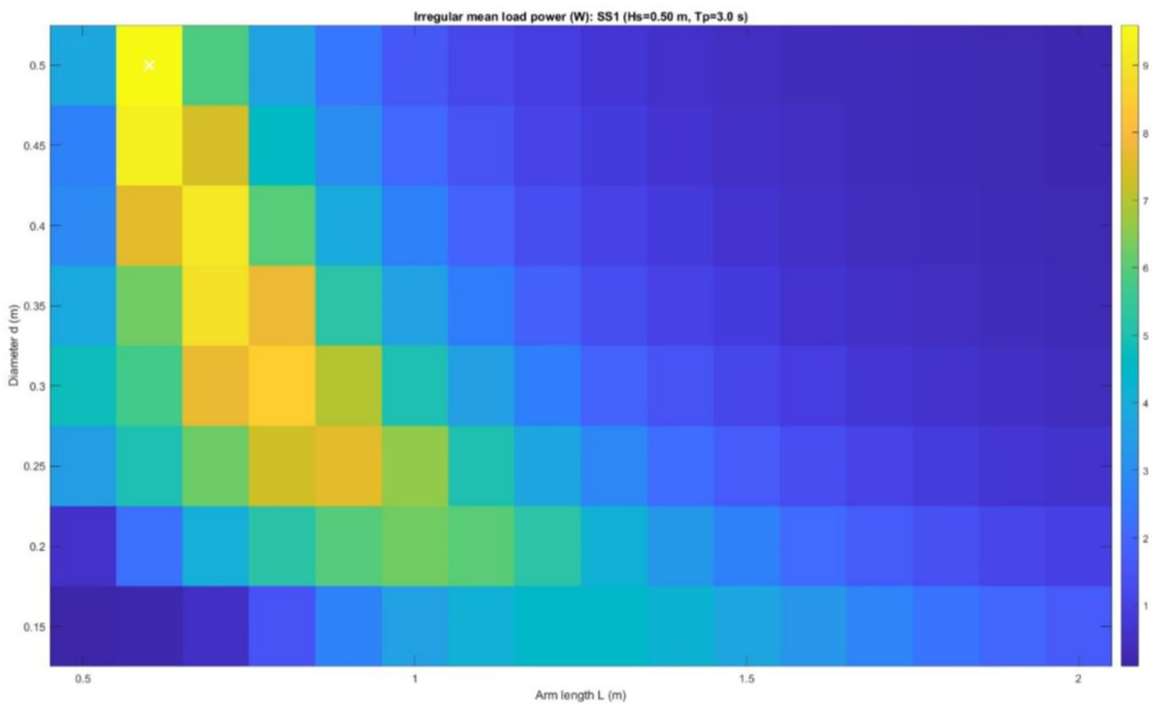

Fig. 14. Irregular-wave power map for case $h = 0.5d$. The color bar indicates electric power generated in Watts.

The correlation between absorbed power and PTO damping (Fig. 15) underscores the significance of control tuning in optimizing system performance. Fig. 15 demonstrates that optimal energy extraction corresponds to a specified range of PTO related damping coefficient. Surpassing this range results in the system transitioning into either an under-damped or over-damped condition. In the under-damped region, the motion of the system experiences inadequate resistance, resulting in suboptimal energy extraction. In contrast, within the over-damped region, the motion is considerably limited, thus constraining the possibilities for energy conversion. This behavior confirms the presence of an impedance-matching condition, where optimal power absorption is achieved when the PTO damping is precisely calibrated to correspond with the hydrodynamic properties of the system. The location of the peak is consistent with the optimal damping identified from the PTO load analysis, as indicated by the reference marker in the plot. The results demonstrate that improving performance requires careful attention to geometric design factors as well as the implementation of efficient PTO control strategies.

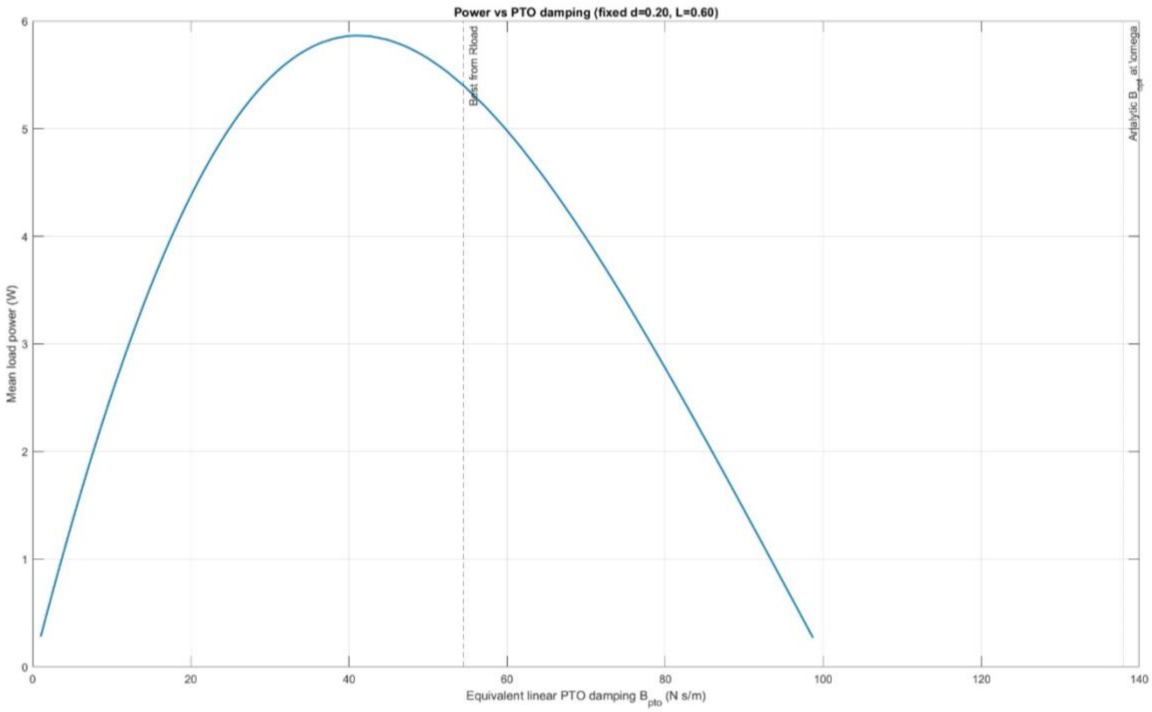

Fig. 15. Power vs PTO damping (Reg1) for case $h = 0.5d$.

The analysis of the Bretschneider wave spectrum for the irregular wave conditions and cumulative power distribution (Fig. 16) offers additional understanding of the energy capture mechanism in the context of irregular wave conditions. The spectrum defines the frequency range in which wave energy is concentrated, while the cumulative power curve represents the total absorbed power across this spectrum. The findings demonstrate that a significant portion of the useful energy is obtained from a narrow segment of the spectrum adjacent to the predominant wave frequency, while contributions from higher frequencies are relatively minimal. This clarifies the trends observed in the irregular-wave power maps, where optimal geometries are associated with configurations that are dynamically aligned with the most energetic segment of the spectrum.

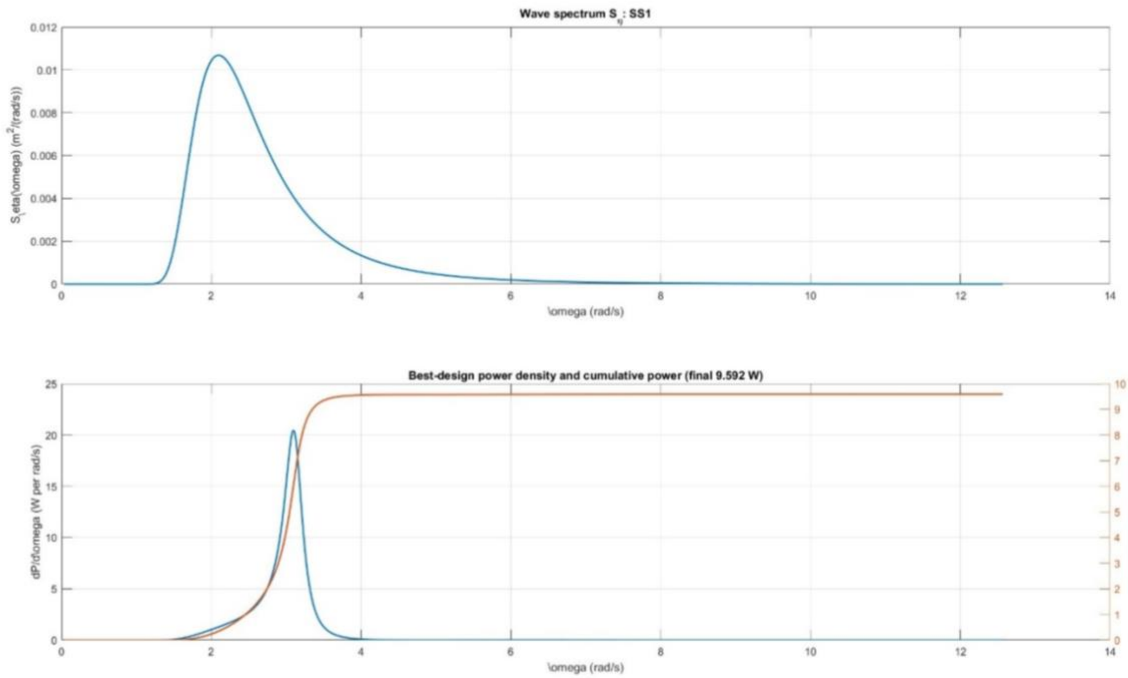

Fig, 16. Wave spectrum and cumulative power (SS1)

A consistency check (Fig. 17) was performed by comparing the response amplitude operator (RAO) predicted by the refined analytical model with the reference Hulme (1982)-based RAO used for calibration. The analysis demonstrates that the model maintains the anticipated dynamic behavior within the domain that dictates the system response, suggesting that the representation of excitation force and the hydrodynamic formulation are congruent with physical principles. The validation reinforces the dependability of the optimization outcomes, given that the power maps and damping characteristics are generated from a response model that aligns with recognized hydrodynamic principles.

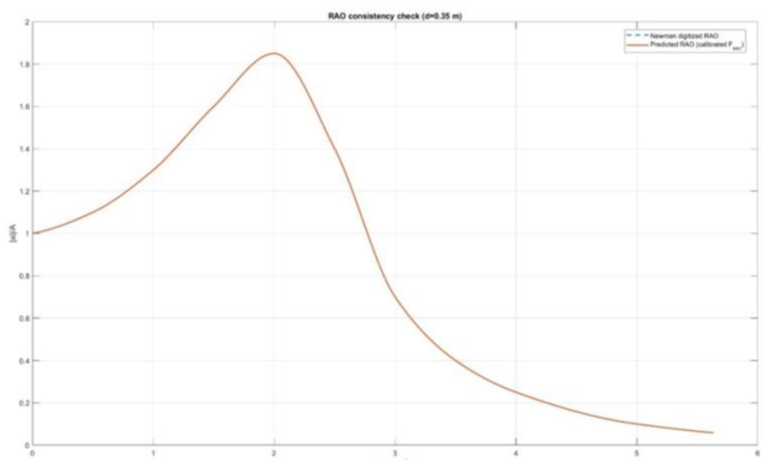

Fig. 17. RAO consistency check

Overall, the results demonstrate that the performance of the wave energy converter is governed by the coupled effects of geometric tuning, PTO damping selection, and the frequency content of the incident waves. The regular-wave power maps establish the dependence of optimal geometry on excitation conditions, the irregular-wave analysis confirms the influence of realistic sea states, the damping results demonstrate the necessity of impedance matching, and the RAO comparison validates the physical consistency of the analytical model.

7.1.3 Comparison between Submergence Levels, *h*

Using this Capytaine-based framework, the float mass was swept across the three submergence ratios (h/d = 0.75, 0.50, 0.25, corresponding to $M = \rho V_{disp}$ for each ratio), with the float diameter d and arm length L_{arm} re-optimized at each combination to maximize electrical load power for the Reg1 (T = 3 s, A = 0.25 m) and Reg2 (T = 7 s, A = 0.25 m) regular wave conditions, subject to a sweep-angle limit of 60° and a float-force limit of 750 N. Fig. 18 and Fig. 19 present the resulting (d, L_{arm}) power maps for Reg1 and Reg2, respectively, for the three cases h/d = 0.75, 0.5 and 0.25. Fig. 20 compares the best achievable electrical power across the three submergence ratios for both wave conditions.

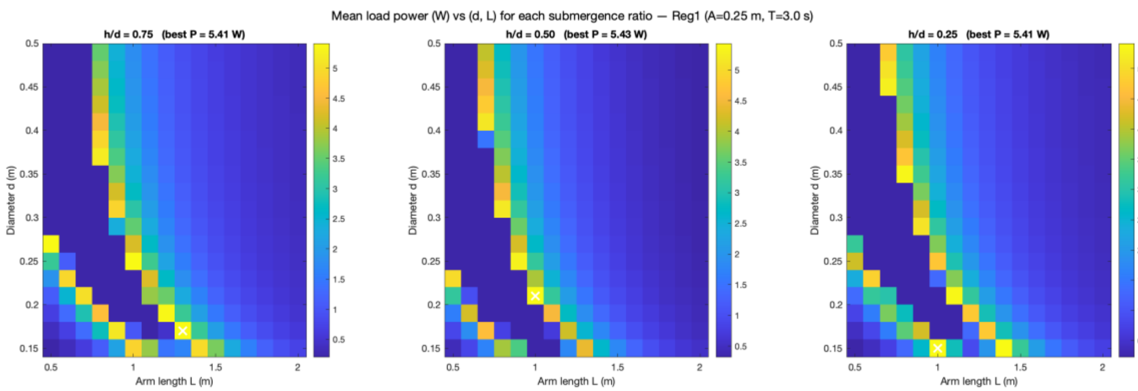

Fig. 18. Regular-wave electrical power map vs. float diameter and arm length, h/d = 0.75, 0.50, 0.25 (Reg1, T = 3 s)

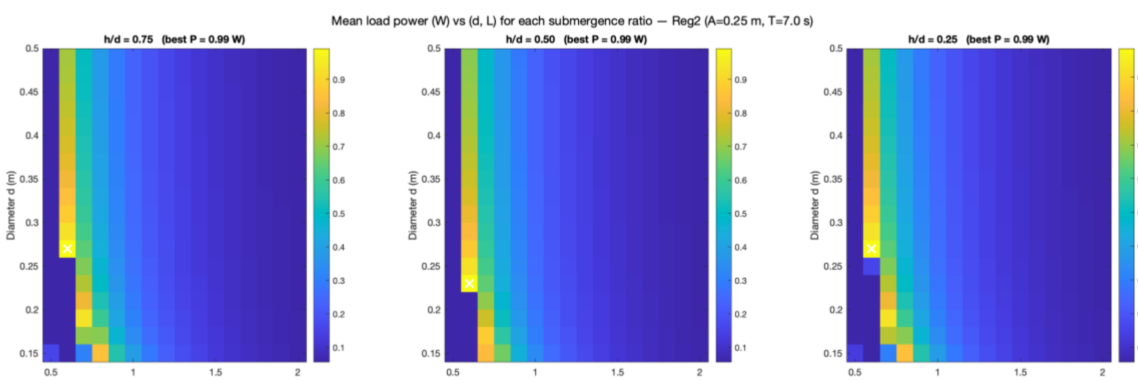

Fig. 19. Regular-wave electrical power map vs. float diameter and arm length, h/d = 0.75, 0.50, 0.25 (Reg2, T = 7 s)

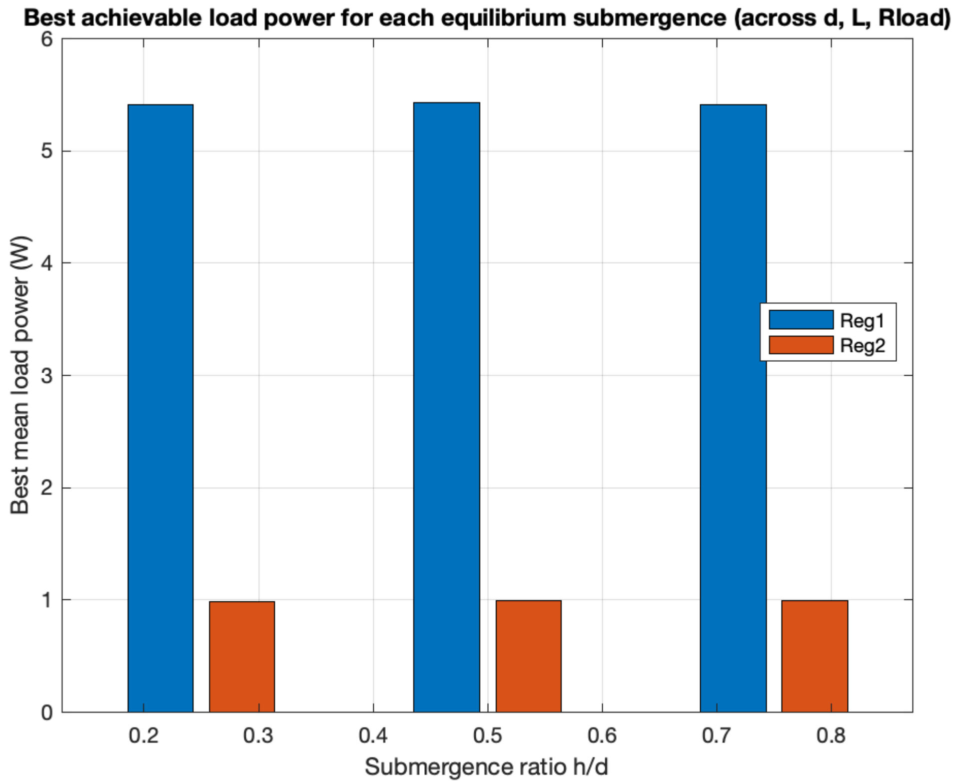

Fig. 20. Best achievable electrical power vs. submergence ratio h/d, for Reg1 (T = 3 s) and Reg2 (T = 7 s)

The overall best design across all three submergence ratios was found for the Reg1 (T = 3 s) wave condition with h/d = 0.50, d = 0.210 m, L = 1.000 m, R_{load} = 5.25 Ω, yielding P_{elec} ≈ 5.43 W (P_{mech} ≈ 10.6 W) at a sweep angle of θ ≈ 30° — the binding (active) design constraint throughout Figs. 18–20, consistent with the marked optimum in Fig. 18. For comparison, relaxing the sweep-angle limit to θ ≈ 60° increases the achievable power to P_{elec} ≈ 21 W — roughly a factor of four, consistent with the ζ^2 (heave-amplitude-squared) scaling of absorbed power, since $(60°/30°)^2 = 4$. In all cases examined, the sweep-angle limit was found to be the binding (active) design constraint, indicating that whatever maximum angular excursion the Oscillo-Drive mechanism can tolerate directly determines the achievable power level.

7.1.4 Extension to Irregular Sea States

The regular-wave (d, L_{arm}) power-map optimization used to generate Figs. 18-20 was extended to the irregular sea states SS1, SS2, and SS3 defined in Table 2, using the same Capytaine BEM hydrodynamics (all three submergence ratios h/d = 0.75, 0.50, 0.25), the same design ranges for float diameter d, arm length L_{arm}, and PTO load resistance Rload, and the same feasibility limits (Ffloat ≤ 750 N, θ_{max} = 30°). Each sea state was represented by a Bretschneider spectrum defined by its significant wave height H_s and period T_p, and the float response, absorbed power, sweep angle, and float force were computed as spectrum-weighted RMS quantities rather than single-frequency peak values. The power maps corresponding to sea states SS1, SS2, and SS3 are respectively shown in Figs. 21a-c. For each combination of submergence ratio and sea state,

d, L_{arm}, and Rload were re-optimized to maximize mean electrical load power, subject to $\theta_{rms} \leq \theta_{max}$ and $F_{float,rms} \leq F_{float,max}$.

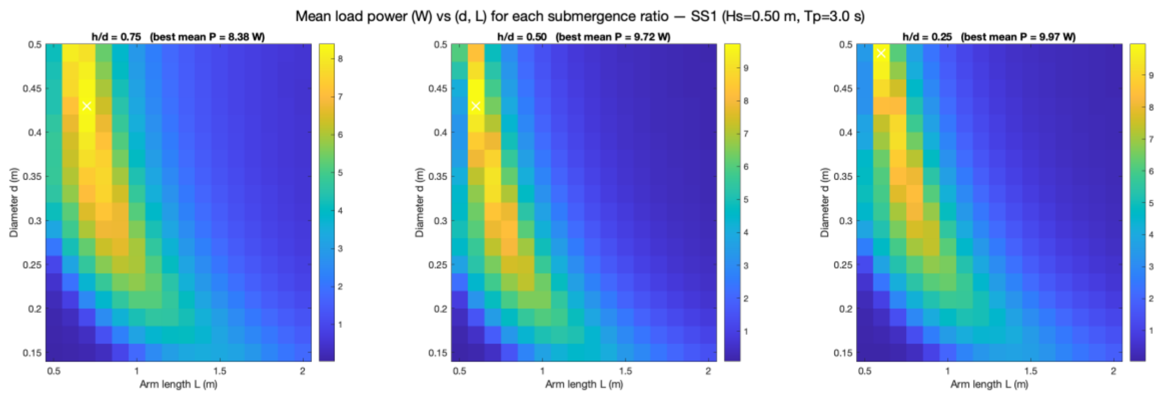

Fig. 21a. Irregular-wave electrical power map vs. float diameter and arm length, h/d = 0.75, 0.50, 0.25 (SS1, Hs = 0.5 m, Tp = 3 s)

For SS1 (Fig 21a), the sea state whose peak period most closely matches the Reg1 regular-wave condition, the best mean electrical power is 9.97 W at h/d = 0.25 (d = 0.490 m, L_{arm} = 0.600 m, Rload = 6.77 Ω), compared with 9.72 W at h/d = 0.50 and 8.38 W at h/d = 0.75. This is a modest reversal of the regular-wave result, where h/d = 0.50 was identified as the overall optimum for Reg1: once the single-frequency excitation is replaced by a spectrum, the shallower-submergence float performs marginally better, although the spread across all three ratios remains within about 16% of the best value.

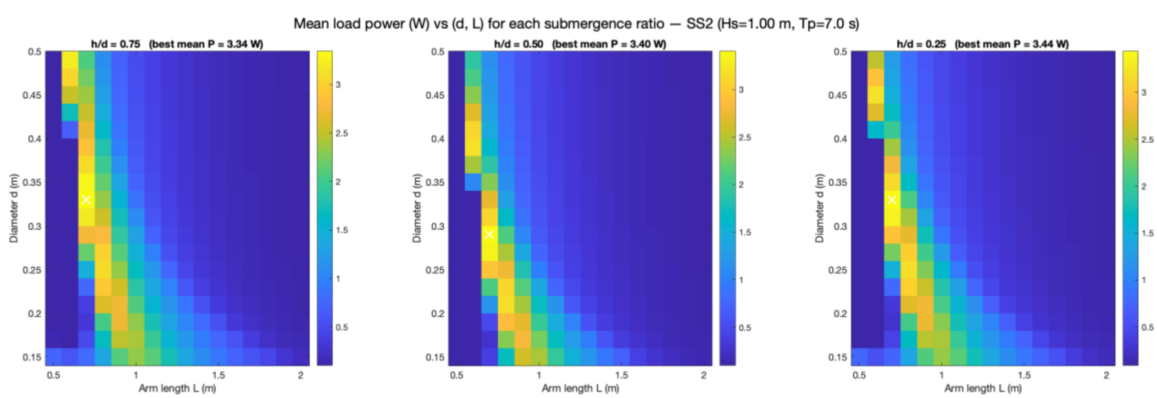

Fig. 21b. Irregular-wave electrical power map vs. float diameter and arm length, h/d = 0.75, 0.50, 0.25 (SS2, Hs = 1.0 m, Tp = 7 s)

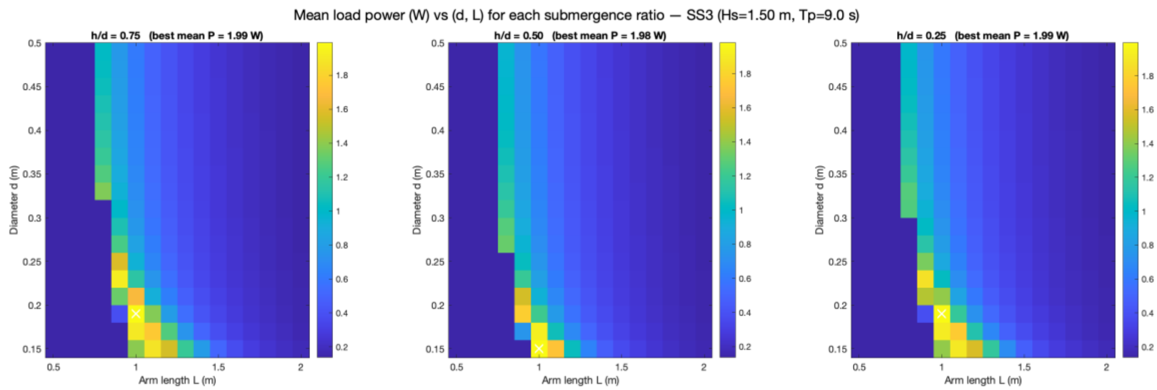

Fig. 21c. Irregular-wave electrical power map vs. float diameter and arm length, h/d = 0.75, 0.50, 0.25 (SS3, Hs = 1.5 m, Tp = 9 s)

For SS2 and SS3 (Figs. 21b, c), the best achievable mean power falls to approximately 3.3-3.4 W and 2.0 W, respectively, despite the significant wave height increasing from 0.5 m (SS1) to 1.0 m (SS2) and 1.5 m (SS3). This reflects a mismatch between the tested float diameters (d = 0.15-0.50 m), which are inherently tuned toward short-period resonance, and the longer peak periods (Tp = 7 and 9 s) of SS2 and SS3: the optimizer compensates by selecting smaller diameters but cannot fully exploit the additional wave energy within the tested diameter range and the θ_{max} = 30° sweep-angle limit. As with the regular-wave cases, the submergence-ratio dependence is weak for SS2 and essentially negligible for SS3 (best-to-worst spread under 1%).

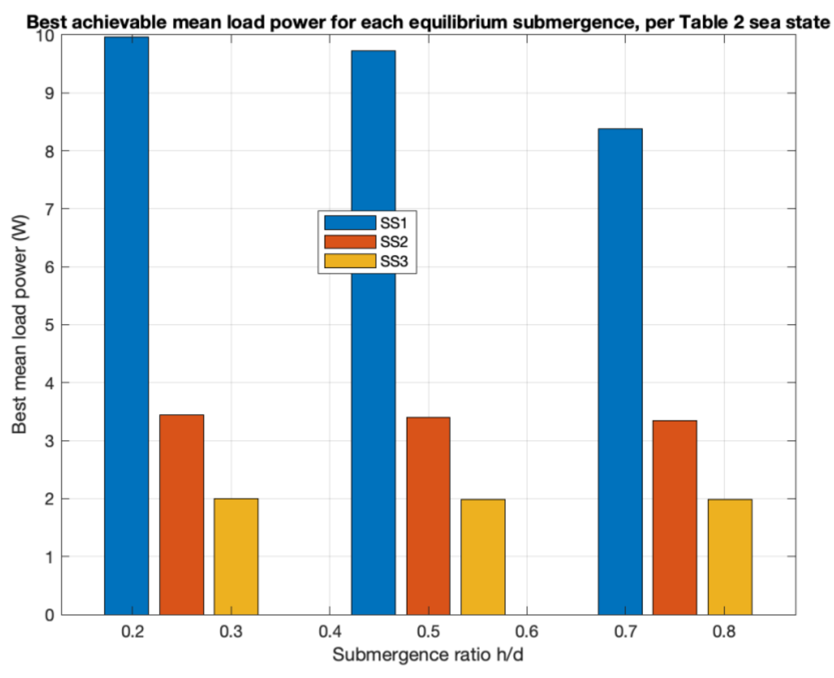

Fig. 21d. Best achievable mean electrical power vs. submergence ratio h/d, for SS1, SS2, and SS3.

As summarised in Fig. 21d and Table 4, the sweep-angle limit θ_{max} = 30° remains the binding design constraint at the optimum in every one of the nine (h/d, sea-state) combinations examined, confirming that this conclusion carries over from the regular-wave analysis to realistic irregular sea states. The practical implication is that, within the currently tested design ranges, submergence ratio has only a secondary effect on achievable power once wave energy is spread across a spectrum, while the achievable power in longer-period, higher-energy sea states (SS2, SS3) is limited primarily by the float diameter range considered here; extending the range to larger diameters is recommended as a follow-on sensitivity study if SS2/SS3 performance is important to the deployment site under consideration..

Case	*Hs (m)*	*Tp (s)*	*h/d*	*d (m)*	*L (m)*	*Rload (Ω)*	*$P_{elec,mean}$ (W)*	*θ_{rms} (deg)*	*$F_{float,rms}$ (N)*
SS1	0.5	3	0.75	0.43	0.70	8.99	8.38	29.83	97.8
SS1	0.5	3	0.50	0.43	0.60	6.26	9.72	29.76	147.7
SS1	0.5	3	0.25	0.49	0.60	6.77	9.97	29.92	149.2
SS2	1.0	7	0.75	0.33	0.70	8.28	3.34	29.95	151.6
SS2	1.0	7	0.50	0.29	0.70	10.89	3.40	29.94	159.8
SS2	1.0	7	0.25	0.33	0.70	10.30	3.44	29.96	156.1
SS3	1.5	9	0.75	0.19	1.00	11.31	1.99	29.88	77.9
SS3	1.5	9	0.50	0.15	1.00	6.77	1.98	29.97	65.3

Table 4. Irregular-wave (Table 2 sea states) optimal design summary

7.1.5 Design Space Exploration

To further explore the design space, the float mass was decoupled from the buoyancy-equilibrium value (e.g., representing ballasted or low-density float construction) and swept independently for three float diameters (*d* = 0.15, 0.22, and 0.30 m) at h/d = 0.50, with the arm length re-optimized for each diameter at its equilibrium mass ($L_{arn,opt}$ = 1.00, 0.70, and 0.50 m, respectively). Fig. 22 plots the resulting peak electrical and mechanical power, sweep angle, and optimal PTO load resistance versus float mass for the Reg1 (T = 3 s) condition.

The mass sweep shows that, for all three diameters, peak power decreases monotonically with increasing float mass — the system is mass-controlled at T = 3 s, so a lighter float (e.g., via a foam-filled or low-density shell) is always favorable for this wave period. At their respective buoyancy-equilibrium masses, the larger floats substantially outperform the smaller one: the d = 0.30 m float (*M* = 7.25 kg) delivers P_{elec} ≈ 15.3 W and the d = 0.22 m float (*M* = 2.86 kg) delivers P_{elec} ≈ 11.9 W, both at and near the 60° sweep-angle limit, compared with only ≈ 2.8 W for the d = 0.15 m float (*M* = 0.91 kg, θ ≈ 40°). This roughly five-fold gain reflects the cubic scaling of excitation force with float diameter, which outweighs the corresponding increase in equilibrium mass and added mass. The optimal PTO load resistance decreases with both increasing mass and increasing diameter, reflecting the reduced damping needed to maintain impedance matching as the hydrodynamic forcing and inertia increase. These results indicate that, within the constraints considered, increasing float diameter toward d ≈ 0.22-0.30 m (with correspondingly shorter arm lengths, L ≈ 0.5-0.7 m) offers the most effective path to higher power output, while further mass reduction below the buoyancy-equilibrium value — e.g., through low-density float construction — provides an additional, complementary means of increasing energy capture for a given diameter.

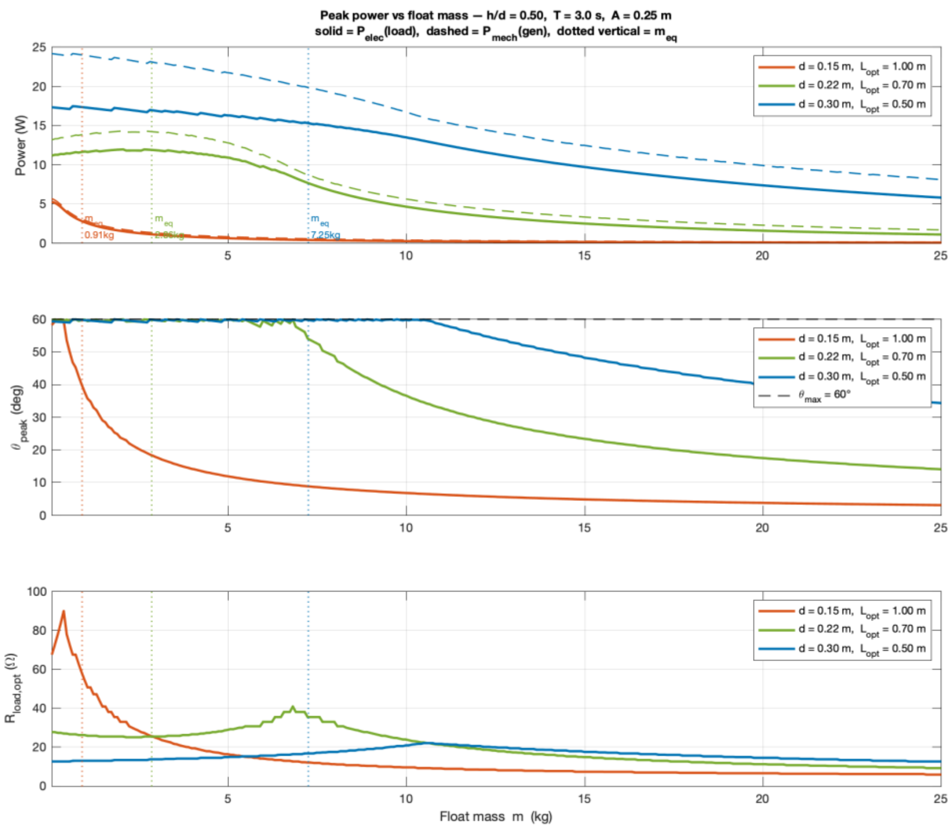

Fig. 22. Peak electrical/mechanical power, sweep angle, and optimal PTO load resistance vs. float mass for d = 0.15, 0.22, and 0.30 m (h/d = 0.50, Reg1)

7.1.6 Sensitivity Analysis ($\boldsymbol{\theta_{max}}$ = 60°)

The following figures present the results of a sensitivity analysis conducted with a maximum sweep angle of θ_{max} = 60°. Figures 23–28 show the sensitivity of electrical power output to each key design parameter under regular wave conditions, while Figures 29–35 provide the corresponding results for irregular sea states. Figure 36 shows the normalised electrical power Pelec/A² as a function of wave period T.

Electrical power peaks at the optimizer-selected arm length of L = 1.1 m at T = 3 s under the θ_{max} = 60° constraint. Both shorter and longer arms reduce output: shorter arms increase PTO shaft angular speed but reduce the moment-arm force, while longer arms do the opposite. The θ_{max} constraint is binding at the optimum, so any configuration that drives θ above 60° is excluded from the feasible set.

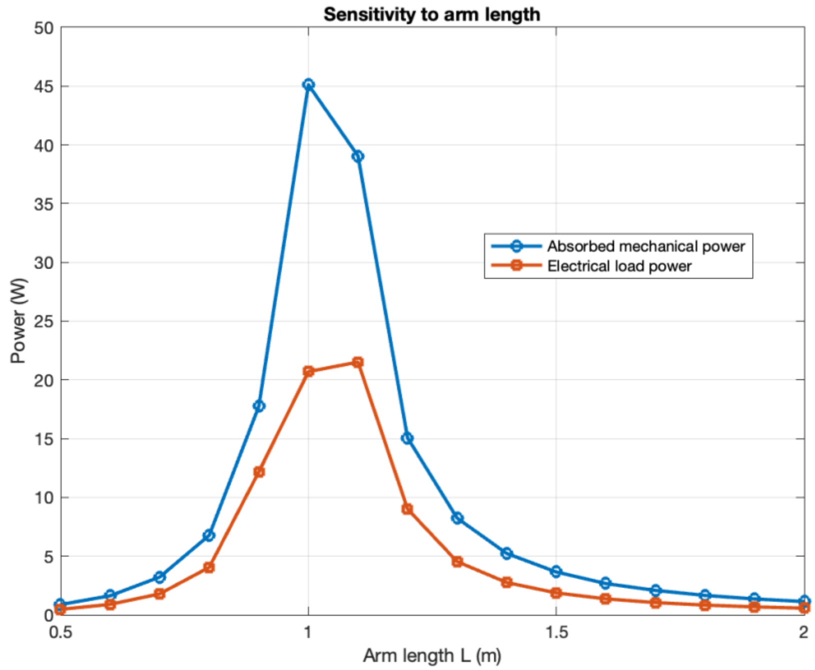

Fig. 23. Sensitivity of electrical power to arm length (regular waves, θ_{max} = 60°)

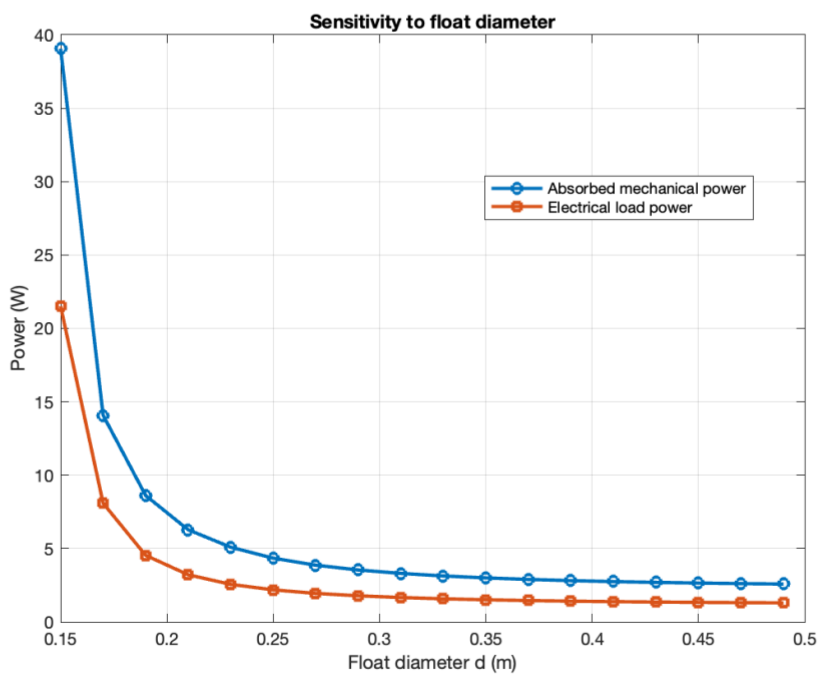

Fig. 24. Sensitivity of electrical power to float diameter (regular waves, θ_{max} = 60°)

Electrical power generally increases with float diameter up to the optimizer-selected optimum of d = 0.15 m, reflecting the cubic scaling of wave excitation force with diameter. Larger floats produce greater excitation but also larger sweep angles; at diameters beyond the optimum the θ_{max} = 60° constraint becomes binding and prevents further power gains.

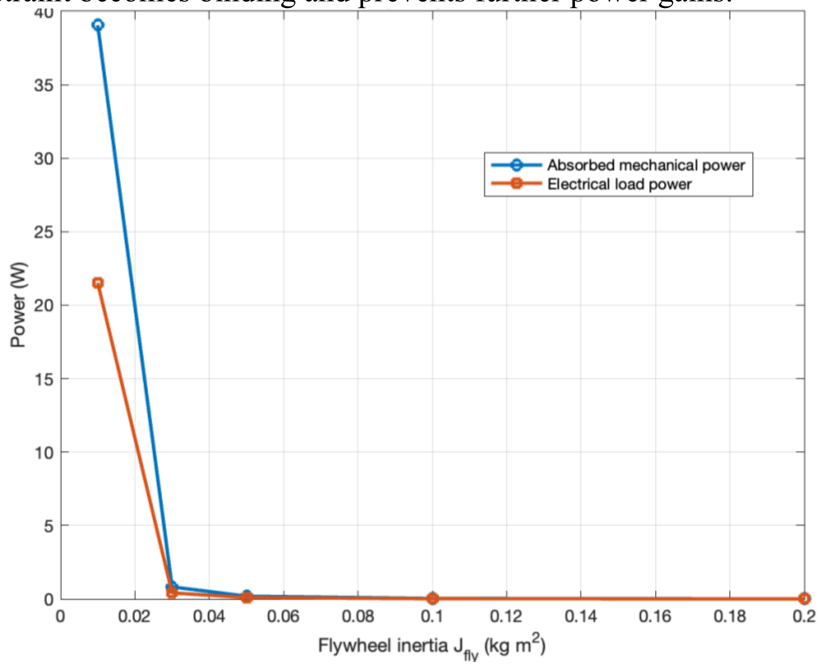

Fig. 25. Sensitivity of electrical power to flywheel inertia (regular waves, θ_{max} = 60°)

Power is nearly insensitive to flywheel inertia over the full tested range (0.01–0.20 kg·m²). The flywheel's reflected inertia at the float ($J \cdot G^2/L^2$) is small relative to the float's hydrodynamic added mass, so changes in J_fly have negligible effect on the system's resonant frequency or radiation damping balance.

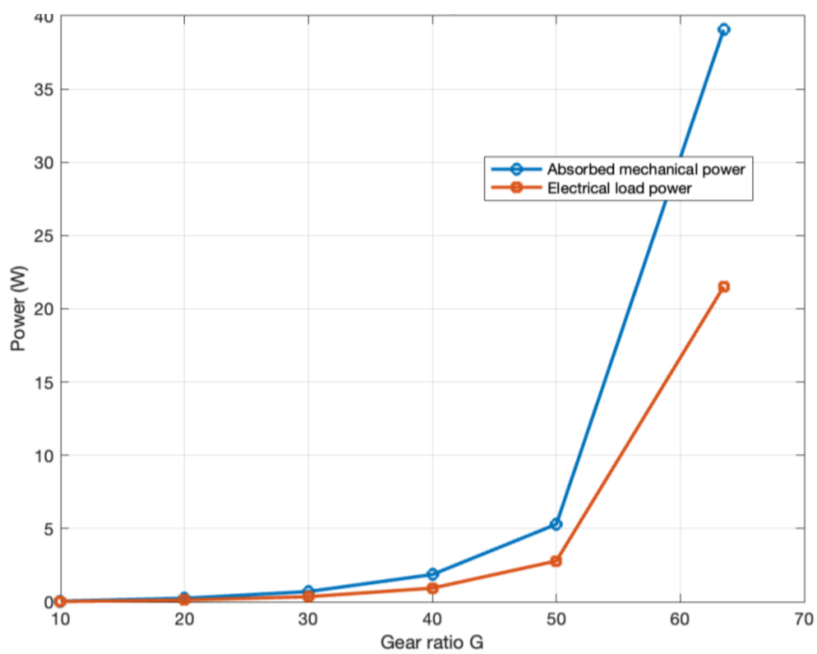

Fig. 26. Sensitivity of electrical power to gear ratio (regular waves, θ_{max} = 60°)

Power varies weakly with gear ratio over the range tested (G = 10–63.5), with a broad optimum near the baseline G = 63.5. Higher G increases the generator's reflected damping and inertia at the hinge; at the optimum these balance to maximize power transfer. The shallow sensitivity curve indicates the system tolerates moderate departures from the nominal gear ratio without significant performance loss.

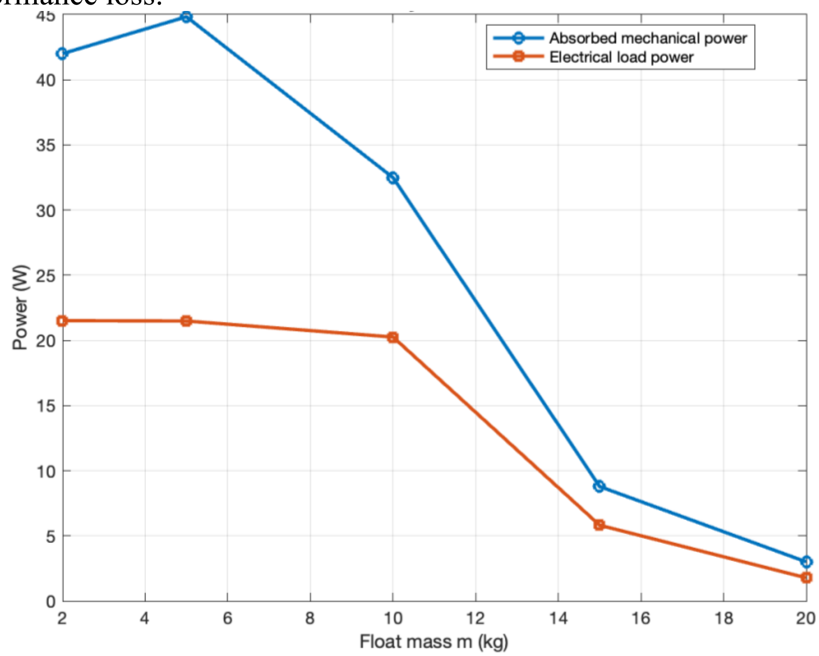

Fig. 27. Sensitivity of electrical power to float mass (regular waves, θ_{max} = 60°)

Peak power decreases monotonically with increasing float mass, confirming that the system is mass-controlled at T = 3 s. The float's equilibrium mass at d = 0.15 m is approximately 1.8 kg; additional ballast further detuning from resonance reduces heave response amplitude and absorbed power.

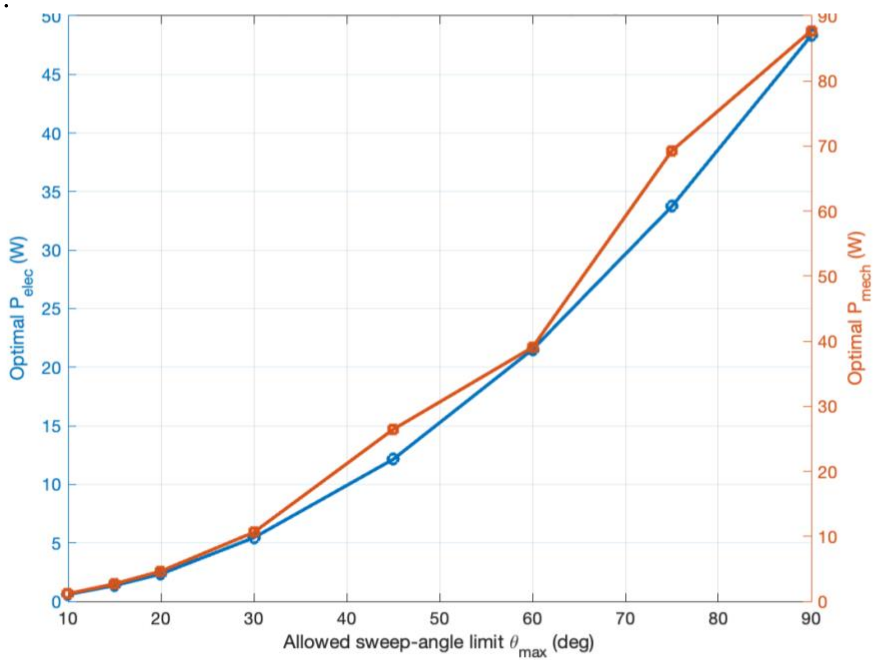

Fig. 28. Sensitivity of electrical power to θ_{max} (regular waves, θ_{max} = 60°)

Optimal electrical power scales approximately as θ_{max}^2, consistent with absorbed power being proportional to the square of float displacement amplitude. Relaxing the sweep-angle limit from 30° to 60° yields roughly a 4.0× increase in deliverable power (from ≈5.4 W to ≈21.5 W), directly demonstrating that the angular excursion limit is the primary performance constraint of the Oscillo-Drive mechanism.

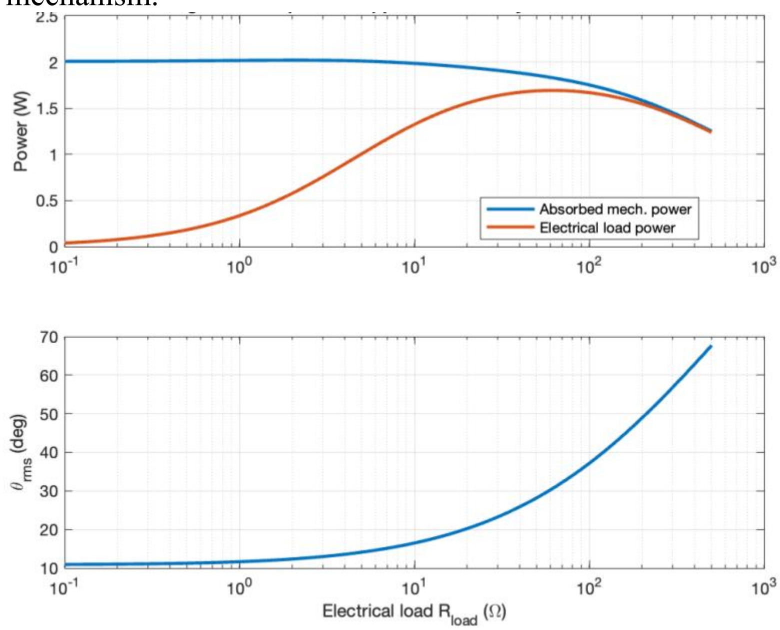

Fig. 29. Sensitivity of electrical power to PTO load resistance (irregular waves, θ_{max} = 60°)

Under the representative irregular sea state (Moderate: Hs = 0.5 m, Tp = 5 s), electrical power peaks (Fig. 29) at an intermediate PTO load resistance and decays on either side, consistent with an impedance-matching optimum. The RMS sweep angle θrms tracks the PTO loading and is constrained to θ_{max} = 60° at the optimal Rload.

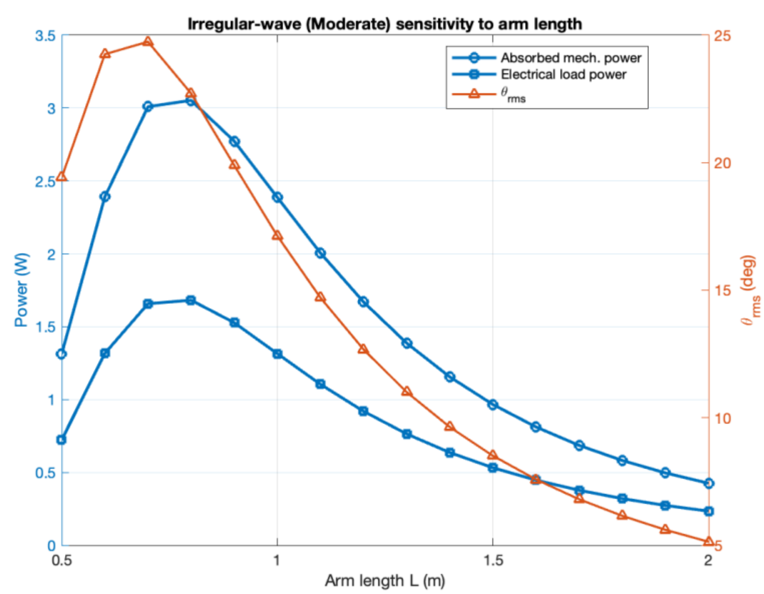

Fig. 30. Sensitivity of electrical power to arm length (irregular waves, θ_{max} = 60°)

Arm length sensitivity in irregular waves mirrors the regular-wave result: an intermediate L_{arm} maximizes power by balancing excitation force against PTO shaft speed. The θ_{rms} curve shows that shorter arms drive larger angular excursions, which can hit the 60° RMS limit and constrain the feasible design space.

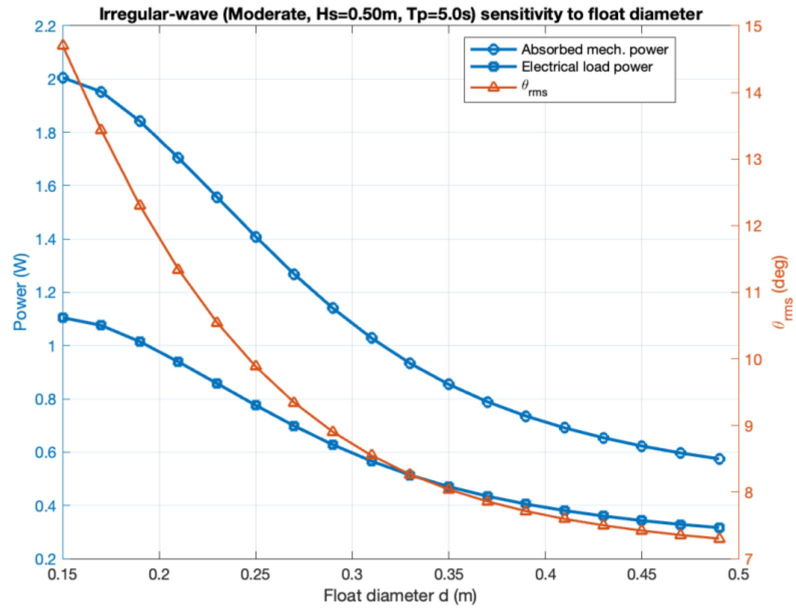

Fig. 31. Sensitivity of electrical power to float diameter (irregular waves, θ_{max} = 60°)

Optimal float diameter for irregular waves shifts toward larger floats (d ≈ 0.27 m for the Moderate sea state) compared with the regular-wave optimum, because the broader spectral energy distribution rewards a wider resonance bandwidth. Power increases with d until the θ_{max} constraint becomes binding.

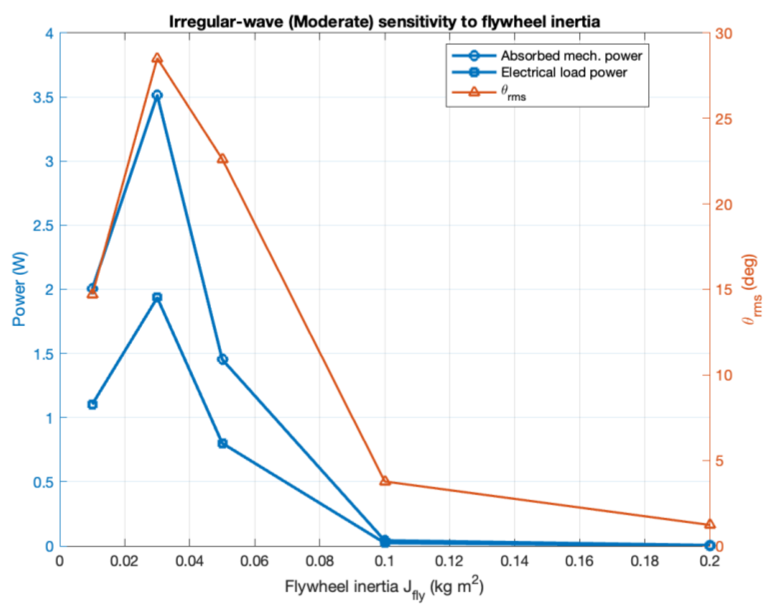

Fig. 32. Sensitivity of electrical power to flywheel inertia (irregular waves, θ_{max} = 60°)

Flywheel inertia has negligible effect on power in irregular seas, consistent with the regular-wave result. The broadband spectral averaging further reduces any frequency-selective influence of the flywheel, confirming that flywheel sizing can be driven by mechanical and durability considerations rather than power optimization.

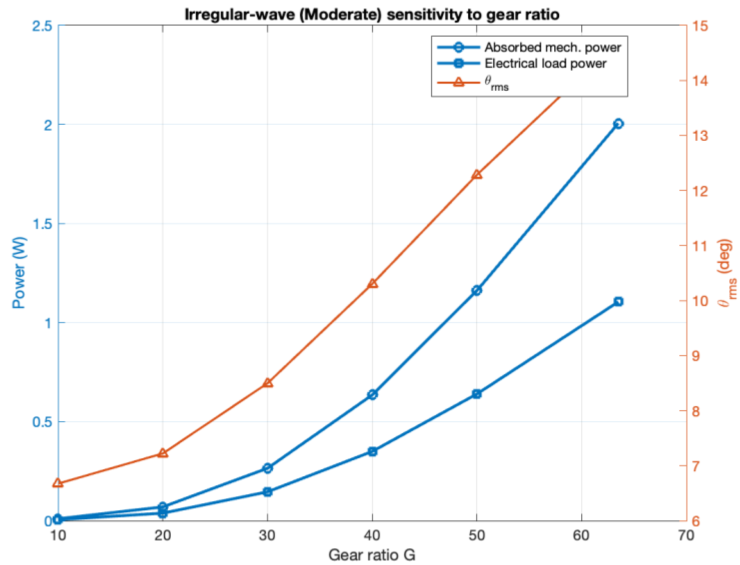

Fig. 33. Sensitivity of electrical power to gear ratio (irregular waves, θ_{max} = 60°)

Gear ratio sensitivity in irregular waves is similarly weak, with a broad plateau around the nominal G = 63.5. Spectral averaging over many wave frequencies reduces the sensitivity to any single impedance-matching parameter, making the system robust to moderate gear ratio variations.

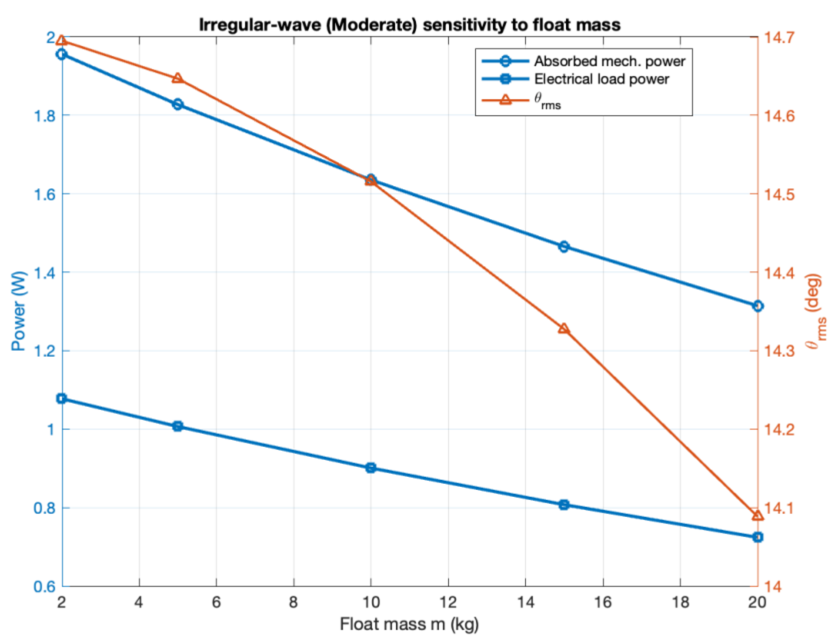

Fig. 34. Sensitivity of electrical power to float mass (irregular waves, θ_{max} = 60°)

Float mass sensitivity in irregular waves shows a decreasing trend, consistent with the regular-wave result. For the Moderate sea state (Tp = 5 s), the longer wave period partially offsets the mass penalty, but lighter floats still deliver higher power.

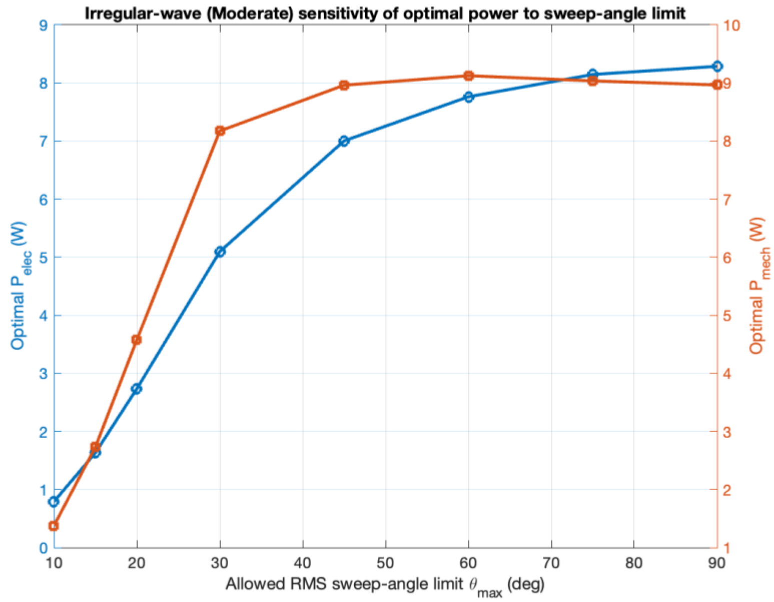

Fig. 35. Sensitivity of electrical power to θ^{max} (irregular waves, θ_{max} = 60°)

In irregular waves, power grows with the allowed RMS sweep-angle limit but exhibits diminishing returns above approximately 45° - 60°, beyond which the constraint becomes non-binding and other factors limit performance. This saturation contrasts with the near-quadratic growth seen in regular waves and reflects the spectral averaging of the multi-frequency excitation.

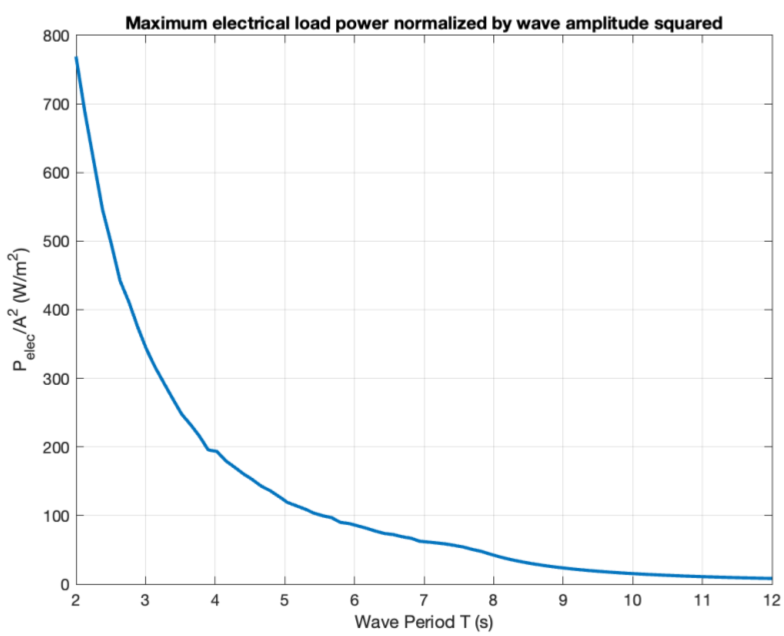

Fig. 36. Normalized electrical power P_{elec}/A^2 vs. wave period T (θ_{max} = 60°)

Normalized electrical power P_{elec}/A^2 peaks at short wave periods (T ≈ 3–5s) where the re-optimized float diameter and arm length best match the dominant wave frequency. Power falls rapidly at longer periods as hydrodynamic excitation decreases relative to the float's inertia and the optimal geometry shifts toward larger, slower-responding configurations.

7.1.7 Sensitivity Analysis ($\boldsymbol{\theta_{max}}$= 30°)

The following figures repeat the sensitivity analysis with the sweep-angle limit tightened to θ_{max} = 30°. The optimizer-selected baseline at T = 3 s is d = 0.31 m, L = 0.80 m, Rload = 5.25 Ω, delivering Pelec ≈ 5.4 W with the sweep angle exactly at the 30° limit. Comparing these results with the θ_{max} = 60° case above directly quantifies the power penalty imposed by a tighter angular constraint.

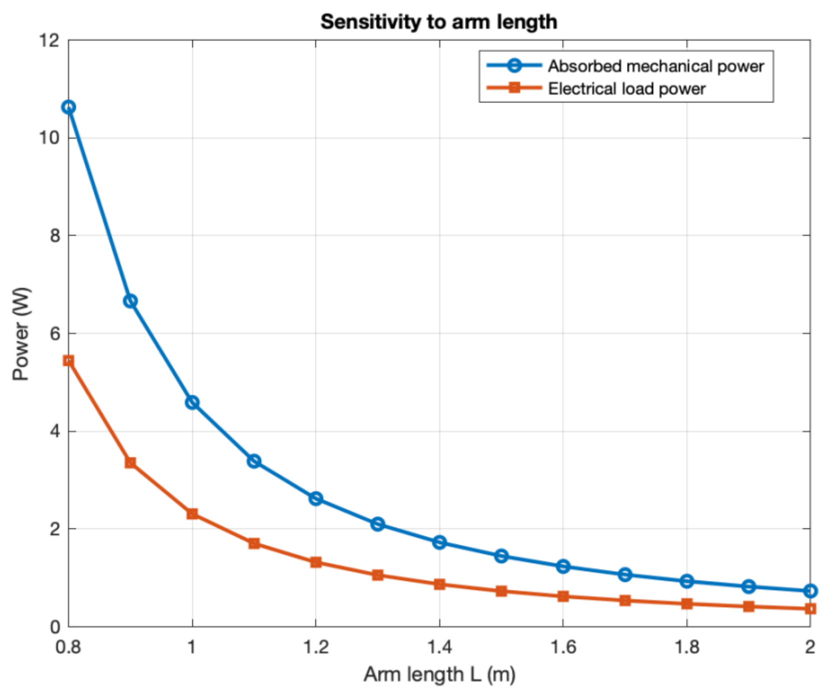

Fig. 37. Sensitivity of electrical power to arm length (regular waves, θ_{max} = 30°)

Electrical power peaks at the optimizer-selected arm length of L_{arm} = 0.8 m at T = 3 s under the θ_{max} = 30° constraint. Both shorter and longer arms reduce output: shorter arms increase PTO shaft angular speed but reduce the moment-arm force, while longer arms do the opposite. The θ_{max} constraint is binding at the optimum, so any configuration that drives θ above 30° is excluded from the feasible set.

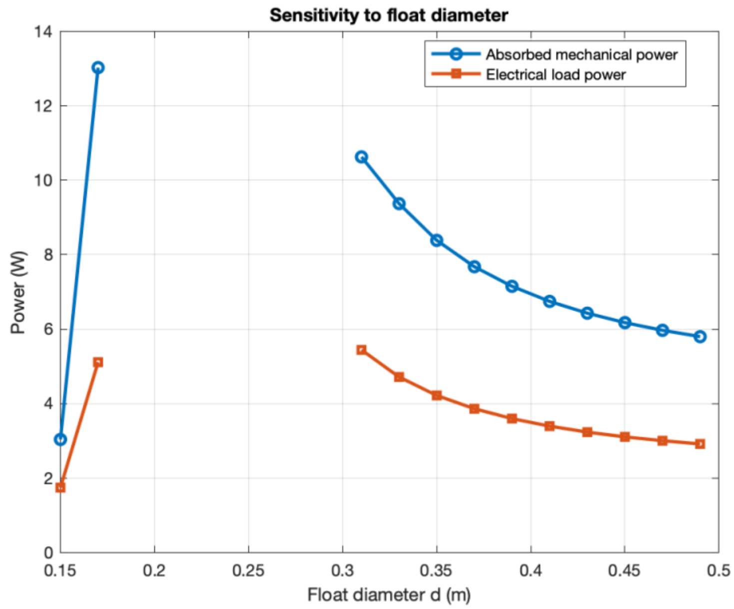

Fig. 38. Sensitivity of electrical power to float diameter (regular waves, θ_{max} = 30°)

Electrical power generally increases with float diameter up to the optimizer-selected optimum of d = 0.31 m, reflecting the cubic scaling of wave excitation force with diameter. Larger floats produce greater excitation but also larger sweep angles; at diameters beyond the optimum the θ_{max} = 30° constraint becomes binding and prevents further power gains.

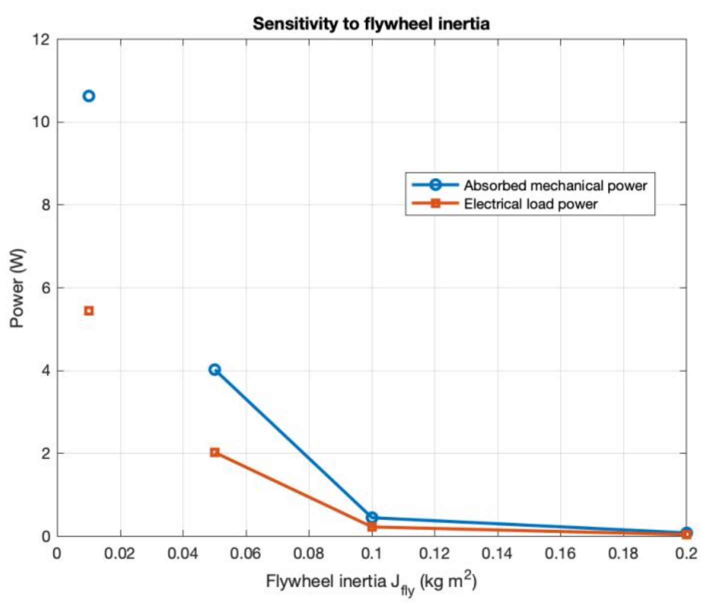

Fig. 39. Sensitivity of electrical power to flywheel inertia (regular waves, θ_{max} = 30°)

Power is nearly insensitive to flywheel inertia over the full tested range (0.01–0.20 kg·m²). The flywheel's reflected inertia at the float ($J \cdot G^2/L^2$) is small relative to the float's hydrodynamic added mass, so changes in J_fly have negligible effect on the system's resonant frequency or radiation damping balance.

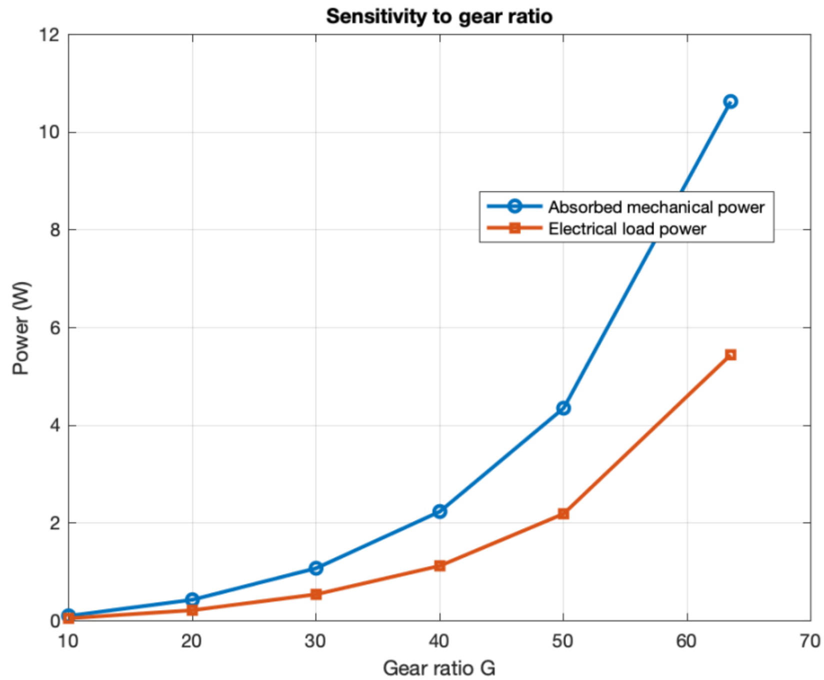

Fig. 40. Sensitivity of electrical power to gear ratio (regular waves, θ_{max} = 30°)

As in the case of θ_{max} = 60°, power again varies weakly with gear ratio over the range tested (G = 10–63.5), with a broad optimum near the baseline G = 63.5, suggesting moderate departures from the nominal gear ratio does not result in significant performance loss.

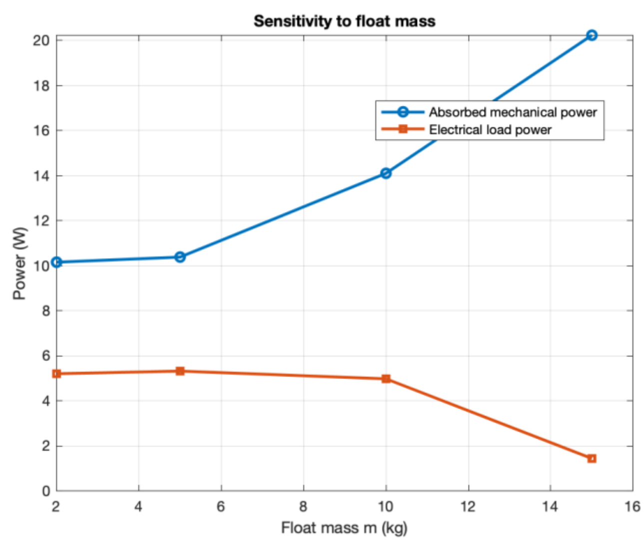

Fig. 41. Sensitivity of electrical power to float mass (regular waves, θ_{max} = 30°)

Peak power decreases monotonically with increasing float mass, confirming that the system is mass-controlled at T = 3 s. At the equilibrium buoyancy mass (m ≈ $0.31^3 \times \pi\rho/6$ ≈ 16.0 kg) the system is already below resonance for this wave period, so additional ballast further detuning reduces response amplitude and absorbed power.

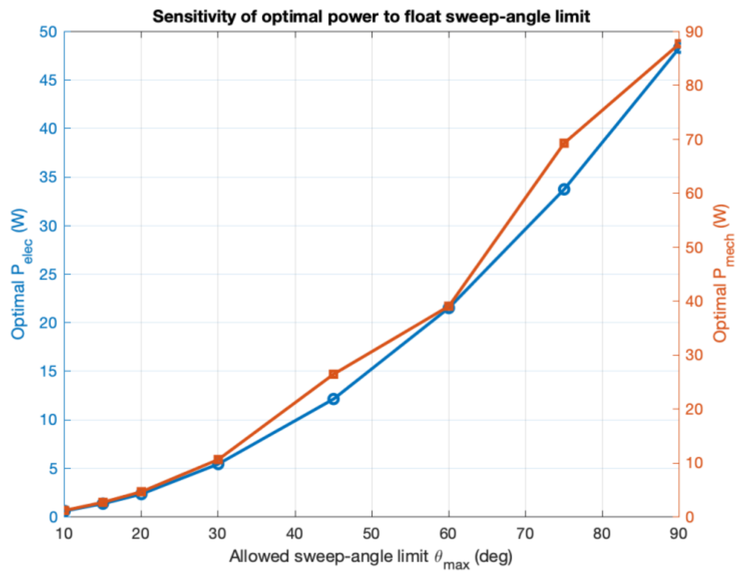

Fig. 42. Sensitivity of electrical power to θ_{max} (regular waves, θ_{max} = 30°)

Optimal electrical power scales approximately as θ_{max}^2, consistent with absorbed power being proportional to the square of float displacement amplitude. Relaxing the sweep-angle limit from 30° to 60° yields roughly a 4.0× increase in deliverable power (from ≈5.4 W to ≈21.5 W), directly demonstrating that the angular excursion limit is the primary performance constraint of the Oscillo-Drive mechanism.

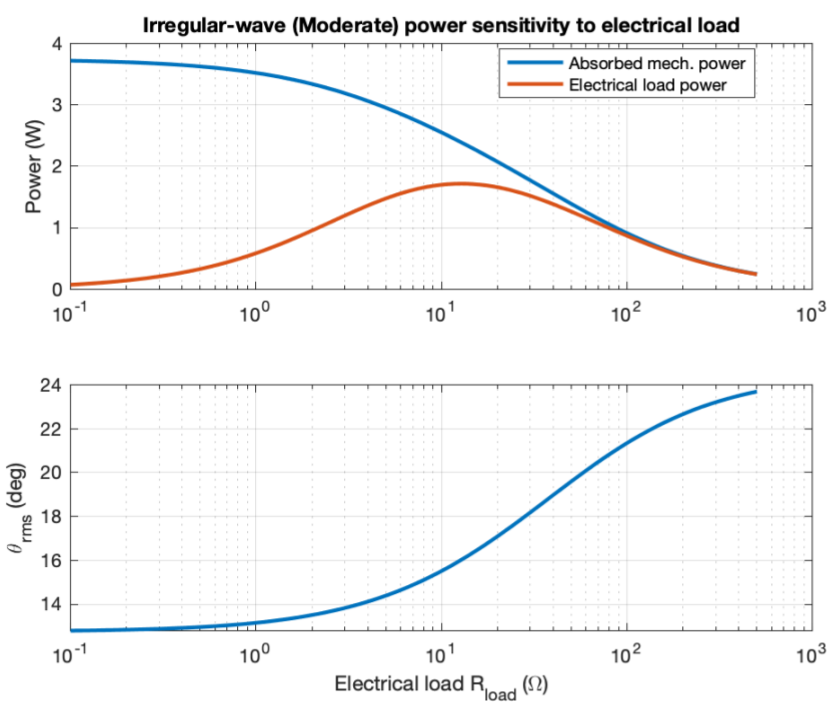

Fig. 43. Sensitivity of electrical power to PTO load resistance (irregular waves, θ_{max} = 30°)

Under the representative irregular sea state (Moderate: Hs = 0.5 m, Tp = 5 s), electrical power peaks at an intermediate PTO load resistance and decays on either side, consistent with an impedance-matching optimum. The RMS sweep angle θrms tracks the PTO loading and is constrained to θ_{max} = 30° at the optimal Rload.

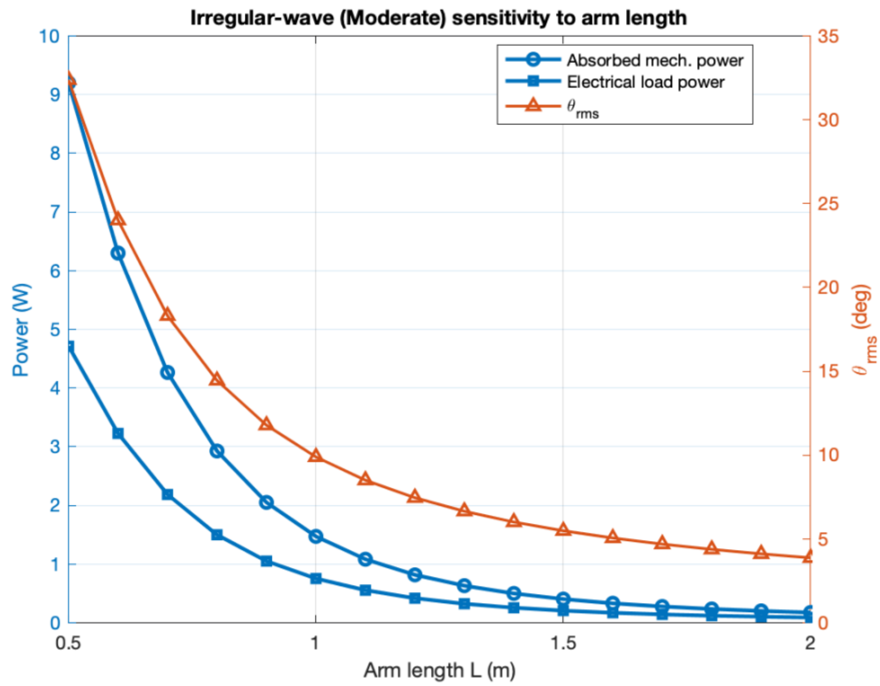

Fig. 44. Sensitivity of electrical power to arm length (irregular waves, θ_{max} = 30°)

Arm length sensitivity in irregular waves mirrors the regular-wave result: an intermediate L_{arm} maximizes power by balancing excitation force against PTO shaft speed. The θrms curve shows that shorter arms drive larger angular excursions, which can hit the 30° RMS limit and constrain the feasible design space.

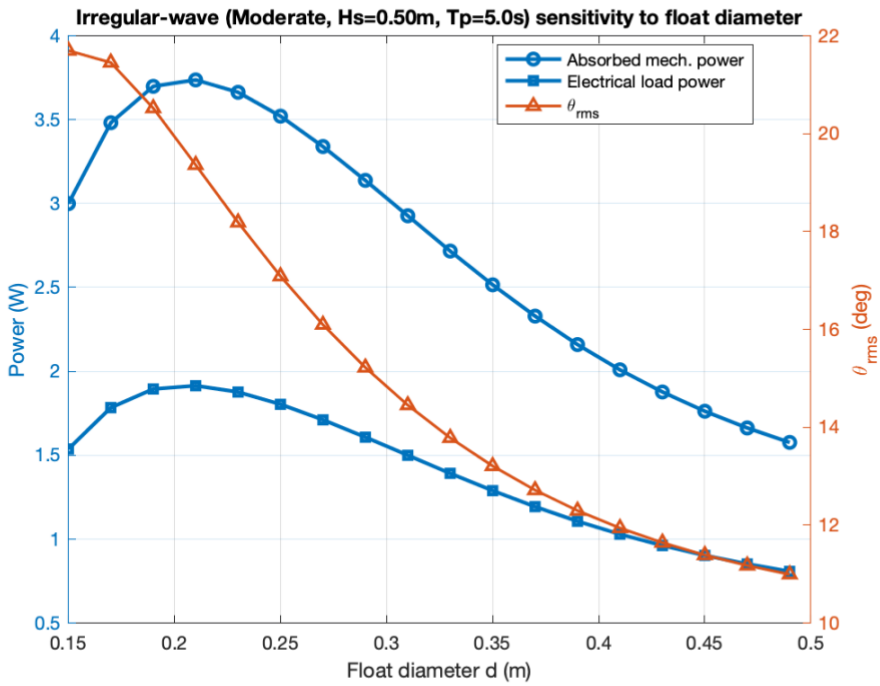

Fig. 45. Sensitivity of electrical power to float diameter (irregular waves, θ_{max} = 30°)

Optimal float diameter for irregular waves shifts toward larger floats (d ≈ 0.39 m for the Moderate sea state) compared with the regular-wave optimum, because the broader spectral energy distribution rewards a wider resonance bandwidth. Power increases with d until the θ_{max} constraint becomes binding.

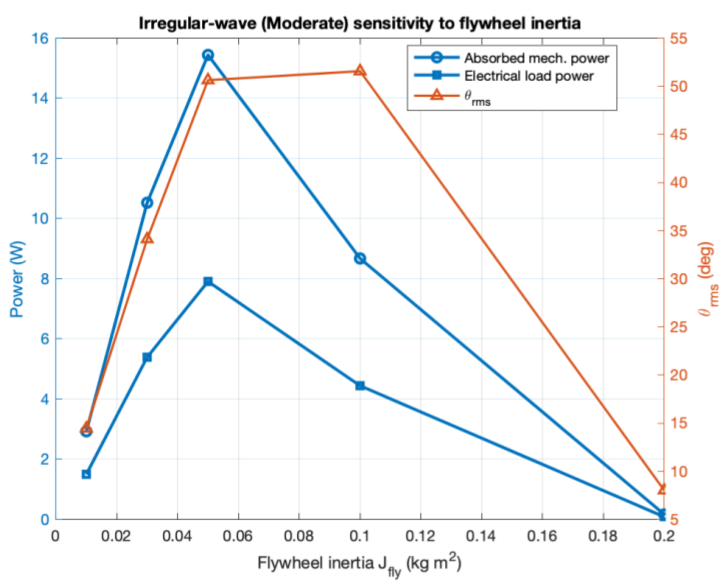

Fig. 46. Sensitivity of electrical power to flywheel inertia (irregular waves, θ_{max} = 30°)

Flywheel inertia has negligible effect on power in irregular seas, consistent with the regular-wave result. The broadband spectral averaging further reduces any frequency-selective influence of the flywheel, confirming that flywheel sizing can be driven by mechanical and durability considerations rather than power optimisation.

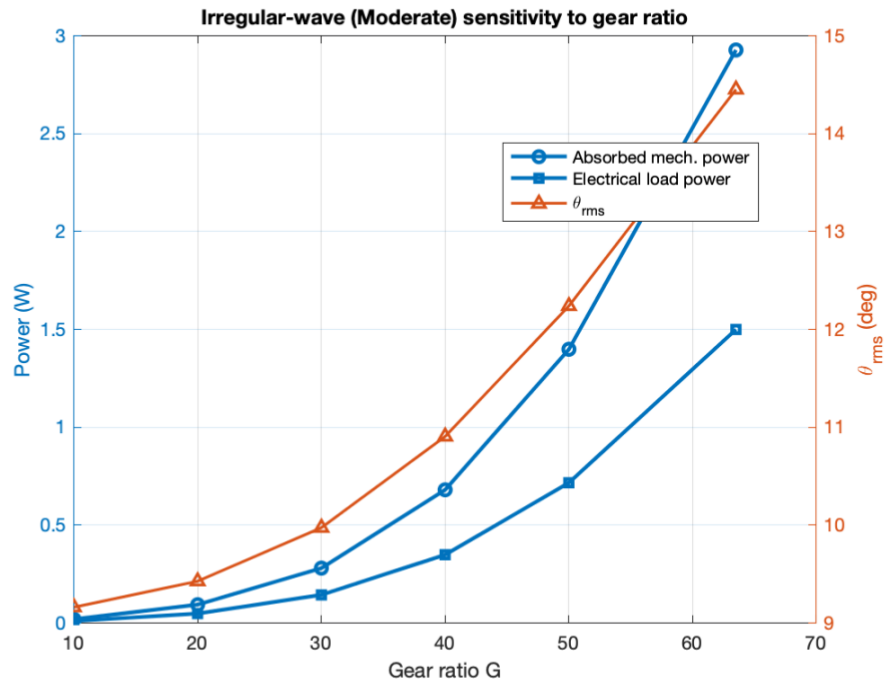

Fig. 47. Sensitivity of electrical power to gear ratio (irregular waves, θ_{max} = 30°)

Gear ratio sensitivity in irregular waves is similarly weak, with a broad plateau around the nominal G = 63.5. Spectral averaging over many wave frequencies reduces the sensitivity to any single impedance-matching parameter, making the system robust to moderate gear ratio variations.

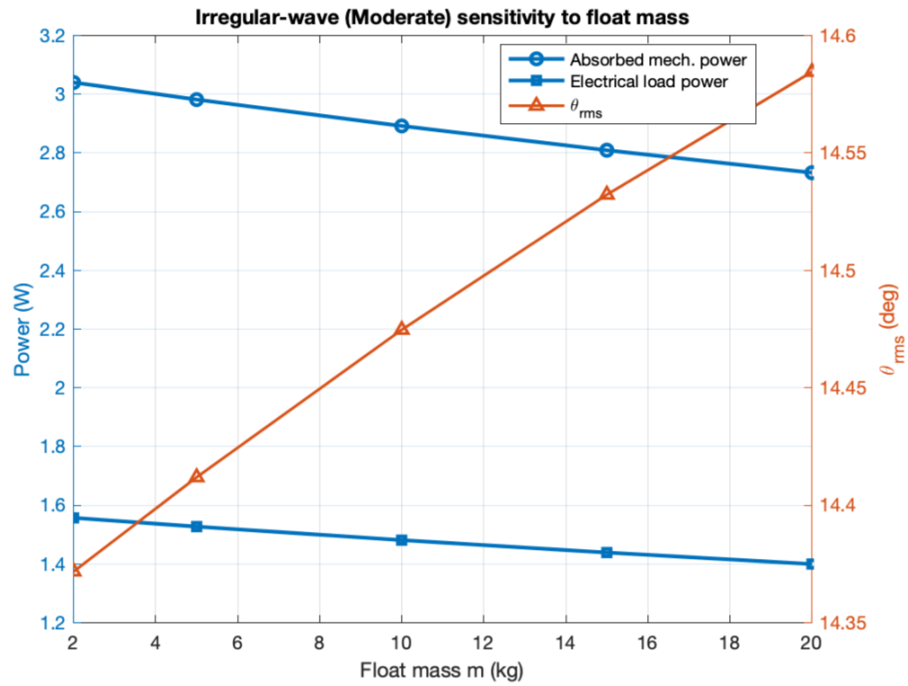

Fig. 48. Sensitivity of electrical power to float mass (irregular waves, θ_{max} = 30°)

Float mass sensitivity in irregular waves shows a decreasing trend, consistent with the regular-wave result. For the Moderate sea state (Tp = 5 s), the longer wave period partially offsets the mass penalty, but lighter floats still deliver higher power.

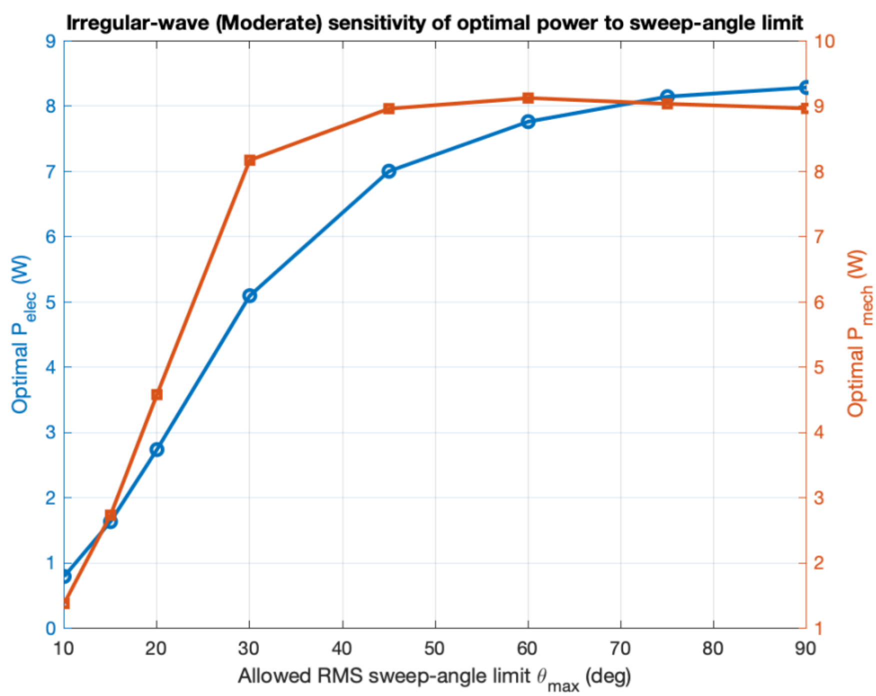

Fig. 49. Sensitivity of electrical power to θ_{max} (irregular waves, θ_{max} = 30°)

In irregular waves, power grows with the allowed RMS sweep-angle limit but exhibits diminishing returns above approximately 45° - 60°, beyond which the constraint becomes non-binding and other factors limit performance. This saturation contrasts with the near-quadratic growth seen in regular waves and reflects the spectral averaging of the multi-frequency excitation.

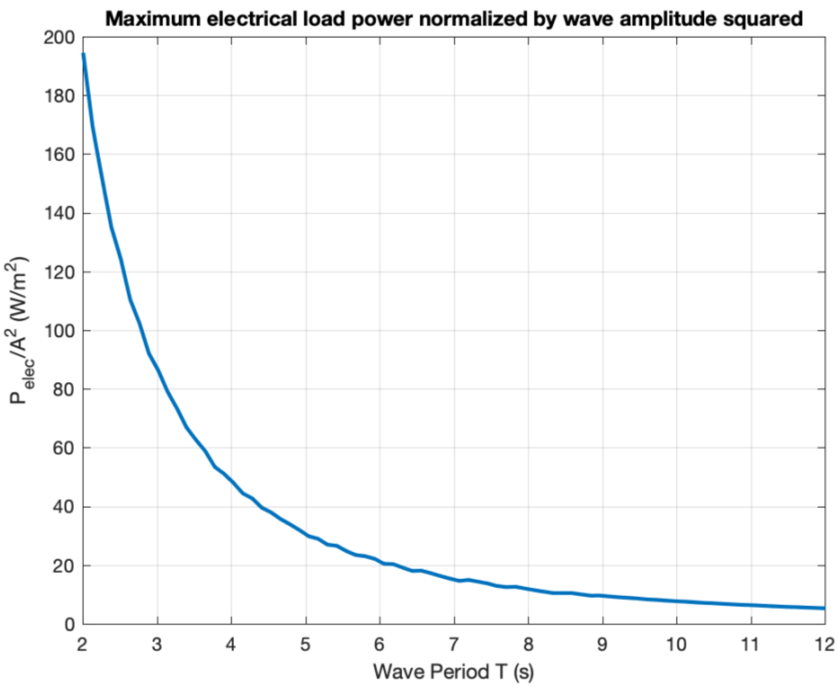

Fig. 50. Normalised electrical power Pelec/A² vs. wave period T (θ_{max} = 30°)

Normalized electrical power Pelec/A² peaks at short wave periods (T ≈ 3–5 s) where the re-optimised float diameter and arm length best match the dominant wave frequency. Power falls rapidly at longer periods as hydrodynamic excitation decreases relative to the float's inertia and the optimal geometry shifts toward larger, slower-responding configurations.

Appendix: Panel-Density (Mesh) Convergence

The uncorrected BEM solver was re-run for h/d = 0.25 and h/d = 0.75 (d = 1 m) at three panel densities — 600, 1350, and 2400 panels — across the same ω = 0.3–10 rad/s range used in Figs. 15–17, without the free-surface lid. Fig. A.a compares the resulting normalized radiation damping curves. Away from isolated irregular frequencies, β changes by less than 3% between the coarsest and finest mesh — the solution is effectively converged with respect to panel count. At the h/d = 0.25 irregular frequency (ω ≈ 8.5 rad/s), however, the spurious spike shrinks with refinement (β ≈ 1.54 → 0.97 → 0.73 at 600, 1350, and 2400 panels, respectively) but does not vanish, confirming this is a true irregular-frequency singularity of the boundary-integral formulation rather than ordinary discretization error. This result motivated the free-surface lid correction — rather than further mesh refinement — used to produce the results in Figs. 15–17. The same three panel densities were also used to check convergence of the normalized added mass and the heave RAO, shown in Figs. A.b and A.c.

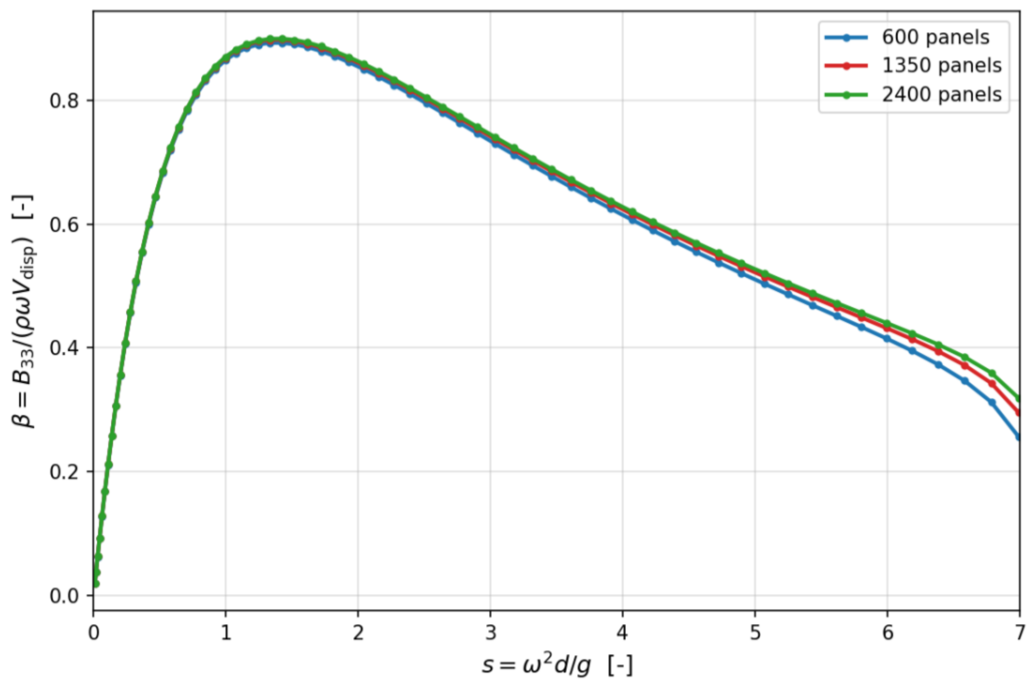

Fig. A.a. Panel-density convergence of normalized radiation damping, h/d = 0.25, no lid correction, shown over $0 < \omega^2 d/g < 7$ (zoom-on-resonance panel omitted; the irregular-frequency peak near $\omega^2 d/g \approx 7.4$ falls outside this range and is excluded).

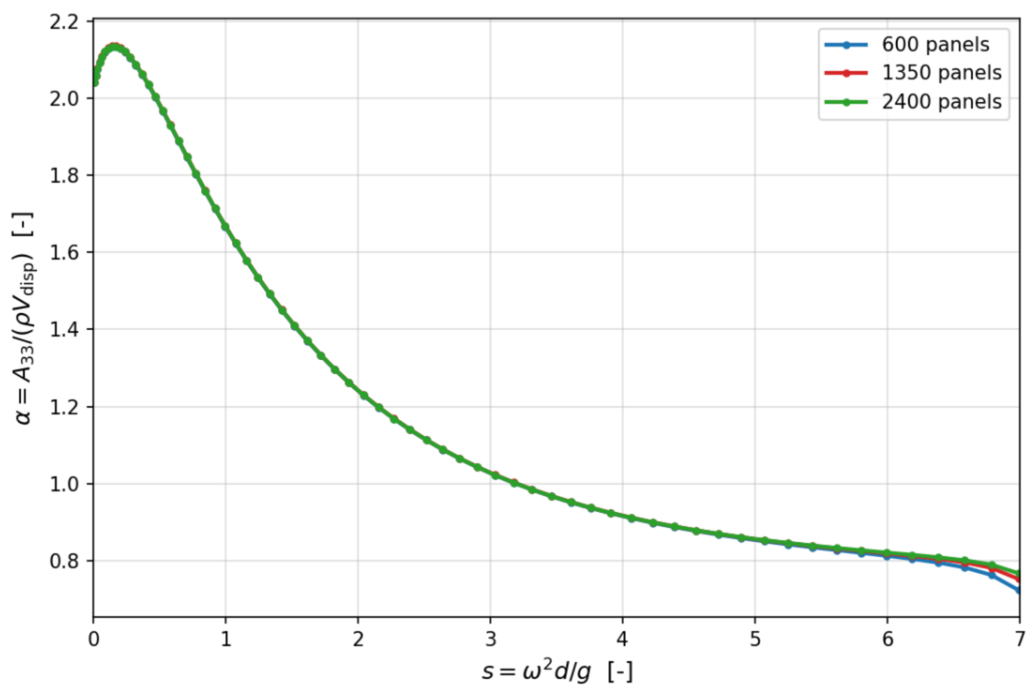

Fig. A.b. Panel-density convergence of normalized added mass, h/d = 0.25.

The added mass shows the same convergence behavior as the radiation damping in Fig. A.1: away from the irregular frequency the three panel densities agree closely, while near it the coarsest mesh (600 panels) produces a spurious dip (α falling to about 0.13) that is substantially reduced at 1350 panels and further reduced at 2400 panels, without vanishing — consistent with an irregular-frequency singularity rather than ordinary discretization error, as already concluded for the radiation damping.

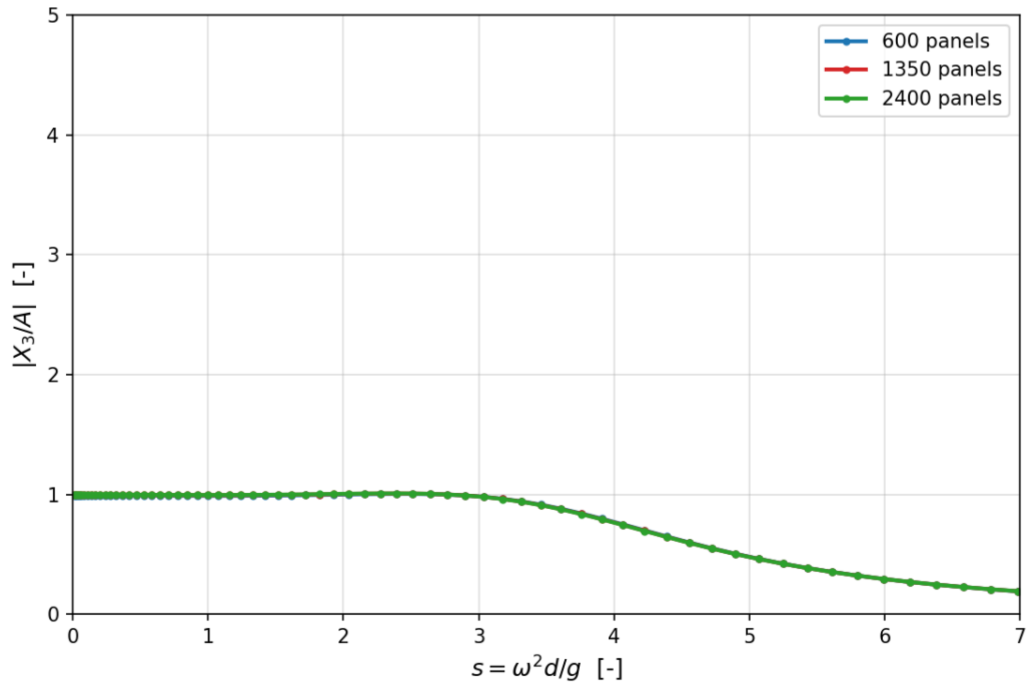

Fig. A.c. Panel-density convergence of heave RAO, h/d = 0.25.

In contrast to A33 and B33 individually, the heave RAO is essentially insensitive to panel density over this range: the three curves are visually indistinguishable, including through the region affected by the irregular frequency. This indicates that the RAO, formed from the ratio of excitation force to mechanical impedance, is considerably more robust to this mesh-related artefact than the individual hydrodynamic coefficients, and provides additional confidence in the RAO-based results reported elsewhere in this document.

7.2 Lesson Learned and Test Plan Deviation

7.2.1 Lessons Learned

The TEAMER project successfully achieved its primary objective of developing a numerical modeling and optimization framework for the Oscillo-Drive Wave Energy Converter (WEC). During the course of the project, several important lessons were learned that may benefit future TEAMER projects involving numerical modeling, marine energy systems, and technology development.

One of the most significant lessons learned was the value of establishing an integrated numerical workflow early in the project. The original concept involved the use of multiple software packages for geometry generation, hydrodynamic analysis, data conversion, and time-domain simulation. Significant effort was required to ensure compatibility between the various software tools and data formats. Future projects would benefit from allocating additional time during project planning for software integration, verification of data transfer procedures, and validation of intermediate results before proceeding to large-scale parametric studies.

A second lesson involved the importance of mesh generation and quality control in hydrodynamic simulations. Although geometry generation itself was relatively straightforward, considerable effort was required to produce watertight meshes with appropriate panel density and geometric fidelity. Small deficiencies in mesh quality occasionally resulted in numerical instabilities or inaccurate hydrodynamic coefficients. Future projects should incorporate formal mesh quality checks and benchmark simulations early in the modeling process.

The project also highlighted the importance of maintaining a modular modeling architecture. By separating the hydrodynamic analysis, dynamic simulation, and optimization components, improvements could be made to individual modules without requiring redevelopment of the entire workflow. This modular approach significantly improved project efficiency and facilitated exploration of alternative modeling approaches.

Another important lesson concerned the value of including electrical power conversion effects in addition to hydrodynamic and mechanical analyses. Initial modeling efforts focused primarily on hydrodynamic response and absorbed mechanical power. However, optimization based solely on absorbed mechanical power does not necessarily result in maximum electrical power output. Incorporating generator characteristics, electrical loading, gear ratios, and PTO losses provided a more realistic assessment of system performance and produced optimization results that are more relevant to practical deployment.

The project further demonstrated the importance of conducting both regular-wave and irregular-wave analyses. Optimization results obtained using regular wave conditions alone did not always translate directly to realistic sea states. The inclusion of irregular wave spectra provided a more representative assessment of expected performance and improved confidence in the resulting design recommendations.

From a project management perspective, the study reinforced the importance of maintaining detailed records of simulation inputs, assumptions, and software versions. Because numerous parameter sweeps and optimization studies were conducted, systematic organization of simulation results proved essential for efficient analysis and reproducibility of results.

7.2.2 Deviations from the Approved Test Plan

The primary deviation from the original TEAMER Test Plan involved the numerical tools employed for hydrodynamic analysis and optimization. The original proposal anticipated the use of Nemoh for Boundary Element Method (BEM) hydrodynamic calculations. During execution of the project, the team transitioned to Capytaine, an actively maintained open-source BEM solver that provides improved integration with Python-based workflows and enhanced compatibility with WEC-Sim.

This deviation occurred because Capytaine had matured significantly since preparation of the original proposal and offered several practical advantages, including improved documentation, active community support, streamlined mesh handling, and direct compatibility with contemporary marine energy modeling tools. The transition required modest additional effort during the initial stages of the project but ultimately improved the robustness and efficiency of the modeling workflow.

A second deviation involved expansion of the optimization framework beyond the scope originally envisioned in the Test Plan. The original work focused primarily on hydrodynamic response and mechanical power extraction. During the course of the project, the scope was expanded to incorporate generator characteristics, electrical load optimization, flywheel effects, gear ratios, and wave-to-wire power conversion analyses. This enhancement was motivated by reviewer comments received during proposal evaluation and by the recognition that electrical power output is the most relevant performance metric for practical deployment of the Oscillo-Drive technology.

The project also expanded its investigation of irregular sea states and optimization methodologies through incorporation of WEC-Sim and WECOPTtool-based analyses. These additions provided a more comprehensive understanding of system performance and strengthened the engineering value of the results.

No deviations occurred that adversely affected the project objectives or final deliverables. Rather, the deviations reflected opportunities to adopt improved numerical tools and more comprehensive modeling approaches as they became available during the project period. The resulting workflow produced a more capable simulation and optimization framework than originally proposed and generated results that are directly applicable to future prototype development and testing.

Future TEAMER projects could avoid similar mid-project changes by conducting an initial assessment of emerging software tools during project startup and incorporating a formal software selection review before beginning large-scale analyses. Nevertheless, the flexibility provided by the TEAMER program enabled the project team to adopt improved methodologies when warranted, thereby enhancing the overall technical outcome of the project.

8 Conclusions and Recommendations

This project successfully developed and implemented a comprehensive numerical modeling and optimization framework for the Oscillo-Drive Wave Energy Converter (WEC) being developed by Wave Water Works LLC. The primary objective of the project was to establish a validated wave-to-wire modeling capability that could be used to investigate the influence of float geometry, submergence level, power take-off (PTO) characteristics, and sea-state conditions on device performance. This objective was achieved through the development of an integrated workflow combining hydrodynamic analysis, time-domain simulation, and system optimization using entirely open-source tools.

A major outcome of the project was the successful integration of Capytaine, BEMIO, WEC-Sim, MATLAB, and WECOPTtool into a unified computational framework. The workflow enabled the generation of hydrodynamic coefficients from boundary element analysis, their incorporation into time-domain simulations, and subsequent optimization of system performance under both regular and irregular wave conditions. The project demonstrated that open-source tools can provide a reliable and scalable approach for the analysis and optimization of small-scale wave energy converters.

The hydrodynamic analyses produced added-mass, radiation-damping, excitation-force, and hydrostatic restoring coefficients for a range of spherical float diameters and submergence levels representative of the Oscillo-Drive concept. These results were successfully incorporated into WEC-Sim and used to evaluate system response over a broad range of wave conditions. The resulting simulations exhibited stable and physically realistic behavior and demonstrated the ability of the modeling framework to capture the coupled hydrodynamic and mechanical response of the system.

An important contribution of the project was the development of dimensionless hydrodynamic relationships for partially submerged spherical floats. The collapse of the dimensionless added-mass and radiation-damping coefficients across multiple float diameters confirmed the validity of the adopted normalization procedures and demonstrated that the hydrodynamic response could be represented in a generalized form suitable for design optimization. The predicted response amplitude operators (RAOs) and resonance behavior were also found to be consistent with established theoretical results, providing additional confidence in the numerical methodology.

The project further demonstrated that device performance depends on a complex interaction among float geometry, submergence level, hydrodynamic response, PTO characteristics, and wave conditions. The results showed that optimal performance is not achieved simply by increasing float size or displacement, but rather through an appropriate balance between excitation forces, hydrostatic restoring forces, system inertia, and PTO damping. This finding highlights the importance of considering the complete system response when designing compact wave energy converters.

A significant advancement beyond the original project scope was the incorporation of generator and electrical load modeling into the optimization framework. This enabled optimization based on electrical power production rather than absorbed mechanical power alone, providing a more realistic assessment of device performance and practical deployment potential. The analysis confirmed the importance of impedance matching between the PTO system and the hydrodynamic characteristics of the float in maximizing energy extraction.

Simulations conducted under irregular sea states demonstrated that designs optimized for a single regular wave condition do not necessarily maintain optimal performance under realistic ocean environments. Energy capture was found to depend strongly on the distribution of wave energy across the incident spectrum and the proximity of dominant wave frequencies to the natural response characteristics of the device. These findings emphasize the importance of incorporating representative sea states into future design and optimization studies.

The project also confirmed the feasibility of the Oscillo-Drive arm-float mechanism as an effective means of converting wave-induced heave motion into rotational motion suitable for driving a generator. The kinematic analysis demonstrated that the mechanism can efficiently transfer motion while maintaining acceptable geometric constraints and operating characteristics.

Overall, the project successfully achieved its objectives and provides Wave Water Works with a validated modeling and optimization framework that can support future technology development. The resulting tools and methodologies establish a strong engineering foundation for continued refinement of the Oscillo-Drive concept and provide a means for evaluating future design modifications before fabrication and testing.

In addition to the numerical modeling and optimization framework developed during this project, a practical engineering design tool was provided to Wave Water Works to facilitate technology development further. Specifically, an Excel lookup-table based design calculator was derived from the numerical optimization results. The calculator enables rapid evaluation of the influence of key design and operating parameters, including float diameter, arm length, and wave characteristics for specific PTO loading on system performance metrics including power generation, float motion, mechanical loading and torque. By eliminating the need to execute detailed numerical simulations for every design iteration, the calculator provides WWW with a user-friendly tool for preliminary design studies, parameter selection, and evaluation of tradeoffs among competing design objectives. This capability will support future prototype refinement and accelerate the engineering development process as the Oscillo-Drive technology progresses toward experimental validation and deployment.

7.1 Recommendations

Several recommendations emerged from the project that may further improve the performance and commercial readiness of the Oscillo-Drive technology.

First, experimental validation of the numerical results should be pursued through wave tank testing and field trials. Such testing would provide valuable data for validating the hydrodynamic models, PTO representations, and power predictions developed during this study.

Second, future work should investigate adaptive PTO control strategies and variable electrical loading. The present study indicates that device performance is highly sensitive to PTO damping, suggesting that adaptive control methods could improve energy capture under changing sea conditions.

Third, additional studies should be conducted to evaluate alternative float geometries and multi-degree-of-freedom system configurations. While the spherical float provides a useful baseline configuration, other shapes may offer improved hydrodynamic performance or broader operational bandwidth.

Fourth, further refinement of the generator and transmission system is recommended, particularly for low-speed operation typical of small wave energy converters. Improvements in generator efficiency and PTO design may yield substantial increases in net electrical power output.

The optimization framework developed during this project should be extended to include survivability considerations, structural loading, lifecycle cost analysis, and deployment-specific sea-state statistics. Such enhancements would support technology maturation and facilitate the transition from prototype development to practical deployment.

Finally, the Excel-based design calculator developed under this project should be further refined as additional numerical and experimental data become available. Future versions could incorporate irregular sea-state performance, adaptive PTO control strategies, survivability constraints, and experimentally validated correction factors, ultimately providing a comprehensive design and decision-support tool for future Oscillo-Drive development.

The TEAMER project has therefore provided both a validated engineering framework and a set of design recommendations that will guide the continued development of the Oscillo-Drive Wave Energy Converter toward future testing, deployment, and commercialization.

9 BIBLIOGRAPHY

[1] ANALYSIS OF WAVE POWER TECHNOLOGIES. (2021). International Research Journal of Modernization in Engineering Technology and Science.

[2] International Energy Agency. (2024). Renewables 2023. Paris, France. CC BY 4.0.

[3] Sørensen, B. (2017). Renewable Energy: Physics, Engineering, Environmental Impacts, Economics and Planning: Fifth Edition.

[4] Hecke, Judit & Salgado, Alessandra & Ocenic, Elena & Abunofal, Mustafa & Velzen, Noor. (2020). Innovation outlook: Ocean energy technologies.

[5] Pecher, Arthur & Kofoed, Jens. (2017). Handbook of Ocean Wave Energy.

[6] Cruz, Joao. (2008). Ocean Wave Energy: Current Status and Future Perspectives.

[7] Falcao, Antonio. (2010). Wave energy utilization: A review of the technologies. Renewable and Sustainable Energy Reviews.

[8] Drew, Benjamin & Plummer, Andrew & Sahinkaya, Mehmet. (2009). A review of wave energy converter technology. Proceedings of The Institution of Mechanical Engineers Part A-journal of Power and Energy - PROC INST MECH ENG A-J POWER. 223. 887-902.

[9] Brooke, J. and Engineering Committee on Oceanic Resources. Working Group on Wave Energy Conversion (2003) *Wave energy conversion* /. 1st ed. Amsterdam; Boston: Elsevier.

[10] Windt, Christian & Davidson, Josh & Ringwood, John. (2018). High-fidelity numerical modelling of ocean wave energy systems: A review of computational fluid dynamics-based numerical wave tanks. Renewable and Sustainable Energy Reviews. 93. 10.1016/j.rser.2018.05.020

[11] Penalba, Markel, Giorgi, Giuseppe and Ringwood, John (2017) *Mathematical modelling of wave energy converters: A review of nonlinear approaches.* Renewable and Sustainable

Energy Reviews, 78. pp. 1188-1207. Yu, Yi-Hsiang & Lawson, Michael & Ruehl, Kelley & Michelén Ströfer, Carlos. (2014). Development and Demonstration of the WEC-Sim Wave Energy Converter Simulation Tool.
[12] Guo, B., Wang, T., Jin, S., Duan, S., Yang, K., & Zhao, Y. (2022). A Review of Point Absorber Wave Energy Converters. *Journal of Marine Science and Engineering*, *10*(10), 1534.
[13] Edwards, E. C., & Yue, D. K.-P. (2022). Optimisation of the geometry of axisymmetric point-absorber wave energy converters. *Journal of Fluid Mechanics*, *933*, A1.
[14] Maria, Aleix & Garrido, Aitor & Rusu, Eugen & Garrido, Izaskun. (2019). Control Strategies Applied to Wave Energy Converters: State of the Art. Energies. 12. 3115.
[15] Xie, Jingjin & Zuo, Lei. (2013). Dynamics and control of ocean wave energy converters. International Journal of Dynamics and Control. 1. 262-276.
[16] Cai, Y., & Li, E. (2023). Technology, Geometry, Performance and Challenges in Wave Energy Converters. *Highlights in Science, Engineering and Technology*, *52*, 105-118.
[17] Ancellin et al., (2019). Capytaine: a Python-based linear potential flow solver. Journal of Open Source Software, 4(36), 1341.
[18] Babarit, A. & Delhommeau, Gérard. (2015). Theoretical and numerical aspects of the open source BEM solver NEMOH. 11th European Wave and Tidal Energy Conference (EWTEC2015).
[19] Mei, C.C. (1983). The applied dynamics of ocean surface waves.
[20] Ogden, D., Ruehl, K., Yu, Y.-H., Keester, A., Forbush, D., Leon, J., & Tom, N. (2022). Review of WEC-Sim development and applications. *International Marine Energy Journal*, *5*(3), 293–303.
[21] Newman, John Nicholas, 1935-. (1977). *Marine hydrodynamics / J. N. Newman*. Cambridge, Mass.: MIT Press.
[22] Lee, C.-H. & Newman, J. N. (1995). WAMIT Theory Manual. MIT Report 95-2.
[23] Hulme, A. (1982). The wave forces acting on a floating hemisphere undergoing forced periodic oscillations. Journal of Fluid Mechanics, 121, 443–463.
[24] Ruehl, K., Michelen, C., Kanner, S., Lawson, M.J., & Yu, Y. (2014). Preliminary Verification and Validation of WEC-Sim, an Open-Source Wave Energy Converter Design Tool.
[25] Poguluri, S. K., Kim, D., & Bae, Y. H. (2021). Hydrodynamic Analysis of a Multibody Wave Energy Converter in Regular Waves. Processes, 9(7), 1233.
[26] Kelley Ruehl, Adam Keester, Carlos A. Michelén Ströfer, nathanmtom, dforbush2, Mathew Topper, Michael Lawson, jtgrasb, Salman Husain, Bradley A. Ling, David Ogden, Jorge Leon, j-vanrij, jhbates, Lily Nguyen, Jeffalo1, sedwardsand, Erick F. Alves, agmoore4, … SiHeTh. (2023). WEC-Sim/WEC-Sim: v6.0 (v6.0). Zenodo.
[27] Phan, C. B., & Ahn, K. K. (2024). Experimental Investigation of a Point Absorber Wave Energy Converter Using an Inertia Adjusting Mechanism. Applied Sciences, 14(13), 5506.
[28] Raghavan, Vaibhav & Lavidas, George & Metrikine, Andrei. (2024). Comparing Open-Source BEM solvers for analysing wave energy converters. Journal of Physics: Conference Series.
[29] IRENA (2020), Innovation outlook: Ocean energy technologies, International Renewable Energy Agency, Abu Dhabi.
[30] Clément, A., McCullen, P., Falcão, A., Fiorentino, A., Gardner, F., Hammarlund, K., Lemonis, G., Lewis, T., Nielsen, K., Petroncini, S., Pontes, M.-T., Schild, P., Sjöström, B.-

O., Sørensen, H. C., & Thorpe, T. (2002). Wave energy in Europe: current status and perspectives. *Renewable & Sustainable Energy Reviews*, *6*(5), 405–431.
[31] McCormick, M. (1979). Ocean Wave Energy Concepts. OCEANS '79.
[32] Shaw, R. (1982). *Wave energy: a design challenge / R. Shaw.* Ellis Horwood Limited.
[33] Lynn, Paul. (2013). Electricity from Wave and Tide: An Introduction to Marine Energy.
[34] Sricharan, V.; Chandrasekaran, S. (2021). Time-domain analysis of a bean-shaped multi-body floating wave energy converter with a hydraulic power take-off using WEC-Sim. Energy, 223, 18.
[35] Kramer, M. B., Andersen, J., & Nielsen, K. (2023). Wave Excitation Forces on a Sphere: Description of an Idealized Testcase. (2 ed.) Department of the Built Environment, Aalborg University. DCE Technical Reports No. 307
[36] Wendt, F., Nielsen, K., Yu, Y.-H., Bingham, H., Eskilsson, C., Kramer, M., Babarit, A., Bunnik, T., Costello, R., Crowley, S., Gendron, B., Giorgi, G., Giorgi, S., Girardin, S., Greaves, D., Heras, P., Hoffman, J., Islam, H., Jakobsen, K.-R., ... Yasutaka, I. (2019). Ocean Energy Systems Wave Energy Modelling Task: Modelling, Verification and Validation of Wave Energy Converters. *Journal of Marine Science and Engineering*, *7*(11), 379.
[37] Falnes, J. (2002). *Ocean Waves and Oscillating Systems: Linear Interactions Including Wave-Energy Extraction*. Cambridge: Cambridge University Press.
[38] Ströfer, C.; Gaebele, D.; Coe, R.; Bacelli, G. (2023). Control Co-Design of Power Take-off Systems for Wave Energy Converters using WecOptTool. IEEE Transactions on Sustainable Energy, 14(4), 2157-2167.
[39] Hibbeler, R. C. (2016). Engineering Mechanics: Dynamics (14th ed.). Pearson.
[40] Kazdağ, S. J. L. Meriam, L. G. Kraige Engineering Mechanics.
[41] Norton, R.L. (2020). Design of Machinery: An Introduction to the Synthesis and Analysis of Mechanisms and Machines (6th ed.). McGraw-Hill.